

SURFACE TEXTURING METHODS FOR THERMOPLASTIC COMPOSITES INJECTION
MOLDING

by

Daniiel Serban



A thesis summary

presented to the Industrial Engineering and Robotics Department

at University "Politehnica" Bucharest

in partial fulfillment of the

thesis requirement for the degree of

Doctor (Ph.D.)

in

Industrial Engineering

Ph.D. Supervisor Prof. Dr. Eng. Ionelia Voiculescu

Bucharest, Romania, 2023

© Daniiel Serban 2023

Abstract

In a speech at National Engineers Week 2000, Neil Armstrong ranked plastics in 20th place, laser and fiber optics 18th, aircraft in third place, cars in second place, and energy supply in the first place, ranking the most significant achievements of the twentieth century. We can say that today, they are more important! Current societal issues include the energy supply crisis, price explosion, plastic recycling, "microplastics," and environmental protection. Injection molding is one of the most used fabrication methods to model thermoplastic composite products at high productivity for transportation or energy industries. The bipolar plates made by injection molding of conductive composites are an alternative to the stainless steel, titan, or graphite ones. Laser machining and additive manufacturing are technologies that have a high scientific and industrial interest. A challenge for Europe is to reduce vehicle fuel consumption and replace fossil fuels with environmentally friendly alternatives. Green Hydrogen fuel cells (PEMFCs) are a possible solution for stationary and mobile applications.

The thesis aims to evaluate texturing technologies of mold cavities and the influence of surface quality and process parameters on physical properties and the replication of the injection molded product. The objectives of research and experiments within the theme were directed towards: advanced manufacturing methods through the evaluation of laser technologies, additive methods for micro surface processing; the influence of surfaces on physical properties; conductive composite materials, evaluation of some applications in the energy industry: injection molded bipolar plates for fuel cells; economic aspects, the assessment of the real possibilities of applying the technological advances obtained through research and development, of "*translation into viable products*" - the development of economic composites of polyolefin matrix (polypropylene and polyethylene) with fillers of carbon black, graphite and testing the product in the functional assembly.

The first part of the thesis includes scientific and technical data related to the current research regarding polymer composite materials, injection molding technology, the typology of injection molds, theoretical aspects related to thermal and electrical conductivity properties (Chapter 1), geometrical particularities of surfaces, the definition of reference terms and notable results regarding the manufacturing technologies of mold cavity surfaces (Chapter 2), with conclusions on the research connected with the thesis theme (Chapter 3). To avoid confusion, we have used the definitions of the terms according to international standards developed by technical committees.

The second part of this work presents the author's original research, experiments, and contributions. Chapter 4 defines the main and specific research objectives, the methodology, the structure of the thesis, the materials, the equipment, and the methodology. Chapter 5 presents the author's contributions to the experimental evaluation of advanced technologies for texturing the mold cavity surfaces and their replication by injection molding. Chapter 6 introduces a milling–laser sequential micromachining system developed by the author and validation of the new method by manufacturing a textured surface of a bipolar plate mold cavity. The experiments of a fuel cell equipped with injection-molded bipolar plates demonstrated the influence of the surface roughness on the electrical contact resistance and fuel cell performance. Further experiments to optimize the process parameters observed that the combined melt and mold temperatures dominated electrical conductivity behavior, and injection pressure was ranked second for polypropylene-graphite composites. Chapters 7 and 8 introduce correlation models for injection pressure estimation and electrical conductivity prediction on a thermodynamic approach.

This summary presents excerpts from the thesis regarding the novelty and originality of the developed methods and materials, the author's research that contributes to improvements in surface texturing, injection molding of the bipolar plates, and industrial integration of the technologies, exemplified in sections 5.4, 6.4 or 6.6.

Thesis Summary Contents

Abstract	i
Thesis Contents	iv
Keywords	vii
<i>Part I Background and Literature Review</i>	
Chapter 1. Polymer matrix composites for injection molding	8
1.5.2 Conductive polymeric composites	8
1.7. Injection molding of thermoplastic composites	9
1.7.10 Applications in the energy industry: bipolar plates for fuel cells	9
Chapter 2. Texturing the mold cavity surfaces	11
2.1. Geometric specification of mold cavities surfaces	11
2.1.1 Surface texture	12
2.1.2. Geometrical specifications of surfaces	12
2.1.3 Correlation Ra – Ch VDI 3400	13
2.1.4. Specifications SPE/SPI	13
2.1.5. Finishing mold cavities surfaces	14
2.2. Subtractive methods for mold cavities surface texturing	14
2.3. Additive manufacturing methods of mold metal cavities	15
2.8 Micromachining research directions	15
Chapter 3. Conclusions regarding the research of surface texturing methods for the injection molding of thermoplastic composite products	16
3.1.1 Properties of thermoplastic composites	16
3.1.2 Testing methods of conductive thermoplastic composite materials	16
3.2 Conclusions regarding surface quality, processing, and generation methods	16
3.3 Micromanufacturing mold surfaces technologies	16
<i>Part II. Contributions</i>	
Chapter 4. Objectives, research methodology, and structure of the doctoral thesis	17
4.1. Surface texturing methods for thermoplastic composites injection molding	17
4.2. The objectives	17
4.3. Directions	17
4.4. Research methodology	17
Chapter 5. Advanced technologies for texturing cavity surfaces and their replication by injection molding	18
5.2 Experiments	18
5.2.1 Model	18
5.2.2 Conductive thermoplastic composites	19
5.2.3 Mold cavities materials	20
5.2.5 Injection molding equipment	20
5.2.6 Metallography analyses equipment	20
5.3 Results and discussions	20
5.3.1 Chemical composition results	20
5.3.2 Photochemical machining method	20
5.3.3 Laser Texturing	22
5.3.4 Additive method – BJT	23

5.3.5 Milling	24
5.3.6 Electrical discharge machining EDM	24
5.3.7 Microhardness analysis of the EDM layer	26
5.3.8 Injection molded surfaces replication	26
5.4 Conclusions on injection mold surfaces finishing	27
5.5 Validation of mold surface manufacturing technologies	28
<i>Chapter 6 Development of sequential milling – laser beam machining system</i>	29
6.2 Description of sequential milling – LBM system adapted to a machining center	29
6.4 2019 MM+LBM Experiments, Results, and Discussion	30
6.4.1 Influence of process parameters on surface roughness	31
6.4.2 Evaluation of injection molded bipolar plates in the fuel cell assembly	31
6.5 2020 MM+LBM Experiments, Results, and Discussion	33
6.5.1 The influence of surface roughness on electrical contact resistance	34
6.5.2 Study of the electrical contact resistance of a BP-GDL assembly	35
6.5.3 Influence of the BP surface quality on the performance of the fuel cell stack	36
6.6 Conclusions regarding the complex laser processing system	36
6.7. Laser processing system validation	37
<i>Chapter 7. Influence of process parameters on the electrical conductivity of injection molded polypropylene-graphite composite products</i>	39
7.2 Materials, Equipment, and Methods	39
7.2.1 Materials	39
7.2.4 Estimate the Injection Pressure Method	39
7.5 Results and discussions	40
7.6 Conclusions regarding the influence of process parameters on the electrical the conductivity of injection-molded products	41
<i>Chapter 8. Thermodynamic evaluation of polymer-carbon hybrid composites conductivity</i>	42
8.3 Results and discussion	42
8.4. Economic highlights	44
8.5. Conclusions regarding the thermodynamic analysis of the conductivity of polyethylene-carbon black-expanded graphite hybrid composites	44
<i>Chapter 9. Conclusions and contributions</i>	45
Bibliography (extras)	47
Published works	48

Thesis Contents

Foreword
Abstract
Nomenclature
<i>Part I Background and Literature Review</i>
Chapter 1. Polymer matrix composites for injection molding
1.1 Plastics and elastomers
1.2. Thermoplastics
1.2.1 Standard thermoplastics
1.2.2 Engineering thermoplastics
1.2.3 High-performance thermoplastics
1.2.4 Thermoplastics of special properties
1.3. Thermosets
1.4. Reinforcing and fillers materials
1.4.1 Reinforcing materials
1.4.2 Fillers
1.4.3 Conductive particulates
1.5. Polymer composites
1.5.1 Reinforced thermoplastics
1.5.2 Conductive polymeric composites
1.6. Test Methods
1.6.1 Mechanical tests
1.6.2 Physical tests
1.6.3 Electrical resistivity, Percolation Threshold
1.6.4 Thermal conductivity
1.6.5 Thermal characterization
1.6.6 Diagrams pVT
1.6.7 Other tests
1.7. Injection molding of thermoplastic composites
1.7.1 Thermoplastics injection molding
1.7.2 Microinjection molding
1.7.3 New injection molding methods
1.7.4 Injection molds
1.7.5 Flow of thermoplastic composites
1.7.6 Demolding
1.7.7 Flow simulation
1.7.8 Statistical methods for optimization of the process parameters
1.7.9 Quality of injection molding products
1.7.10 Applications in the energy industry: bipolar plates for fuel cells
1.8 Recycling
Chapter 2. Texturing the mold cavity surfaces
2.1. Geometric specification of mold cavities surfaces
2.1.1 Surface texture
2.1.2. Geometrical specifications of surfaces
2.1.3 Correlation Ra – Ch VDI 3400
2.1.4. Specifications SPE/SPI
2.1.5. Finishing mold cavities surfaces
2.2. Subtractive methods for mold cavities surface texturing
2.2.1. Materials

2.2.2. Mechanical machining
2.2.3. Abrasive machining
2.2.4. Photochemical machining <i>PCM</i>
2.2.5 Electrical discharge machining <i>EDM</i>
2.2.6 Electrochemical machining <i>ECM</i>
2.2.7 Laser beam machining <i>LBM</i>
2.2.8 Ion beam machining <i>IBM</i>
2.2.8 Electron Beam Machining <i>EBM</i>
2.3. Additive manufacturing methods of mold metal cavities
2.3.1 Metals for additive manufacturing
2.3.2 Binder Jetting <i>BJT</i>
2.3.3 Selective Laser Sintering
2.3.4 Selective Laser Metal Melting
2.3.5 Directed Energy Deposition <i>DED</i>
2.3.6 Buildup welding
2.4 Surface treatments
2.5 Maintenance of textured surfaces
2.6 Surface Integrity
2.7 Surface characterization
2.8 Micromachining research directions
<i>Chapter 3. Conclusions regarding the research of surface texturing methods for the injection molding of thermoplastic composite products</i>
3.1 Thermoplastic composites
3.1.1 Properties of thermoplastic composites
3.1.2 Testing methods of conductive thermoplastic composite materials
3.2 Conclusions regarding surface quality, processing, and generation methods
3.3 Micromanufacturing mold surfaces technologies
<i>Part II. Contributions</i>
<i>Chapter 4. Objectives, research methodology, and structure of the doctoral thesis</i>
4.1. Surface texturing methods for thermoplastic composites injection molding
4.2. The objectives
4.3. Directions
4.4. Research methodology
4.5 Thesis layout
4.6. Materials and equipment
4.6.1 Polymeric composites and constituents
4.6.2 Materials for building the experimental molds cavities
4.7. Manufacturing methods and equipment
4.7.1 Technologies and equipment used for manufacturing the experimental surfaces
4.7.2 Experimental molds manufactured
4.7.3 Injection molding
4.8 Test methods
4.8.1 Mechanical tests
4.8.2 Metallography tests equipment
4.8.3 TGA – thermogravimetric analysis
4.8.4 MFR – Melt Flow Index
4.8.5 Electrical resistance
4.8.6 Electrical resistivity
4.8.7 Thermal conductivity
4.8.8 Fuel cell performance evaluation
4.9 Design of Experiments, Statistic Methods

4.10 Published works list
<i>Chapter 5. Advanced technologies for texturing cavity surfaces and their replication by injection molding</i>
5.1. Technologies for cavity surface texturing
5.2 Experiments
5.2.1 Model
5.2.2 Conductive thermoplastic composites
5.2.3 Mold cavities materials
5.2.4 Tooling
5.2.5 Injection molding equipment
5.2.6 Metallography analyses equipment
5.3 Results and discussions
5.3.1 Chemical composition results
5.3.2 Photochemical machining method
5.3.3 Laser Texturing
5.3.4 Additive method – BJT
5.3.5 Milling
5.3.6 Electrical discharge machining EDM
5.3.7 Microhardness analysis of the EDM layer
5.3.8 Injection molded surfaces replication
5.3.9 Weight evaluation
5.3.10 Electrical rezistivity
5.3.11 Thermal conductivity
5.4 Conclusions on injection mold surfaces finishing
5.5 Validation of mold surface manufacturing technologies
<i>Chapter 6 Development of sequential milling – laser beam machining system</i>
6.1. Hybrid, sequential fabrication systems
6.1.1 Mechanical micromachining
6.1.2 Laser beam machining
6.1.3 Laser-assisted hybrid systems
6.1.4 Sequential micromachining milling - laser
6.2 Description of sequential milling – LBM system adapted to a machining center
6.3 Injection molding experiments
6.4 2019 MM+LBM Experiments, Results, and Discussion
6.4.1 Influence of process parameters on surface roughness
6.4.2 Evaluation of injection molded bipolar plates in the fuel cell assembly
6.5 2020 MM+LBM Experiments, Results, and Discussion
6.5.1 The influence of surface roughness on electrical contact resistance
6.5.2 Study of the electrical contact resistance of a BP-GDL assembly
6.5.3 Influence of the BP surface quality on the performance of the fuel cell stack
6.6 Conclusions regarding the complex laser processing system
6.7. Laser processing system validation
<i>Chapter 7. Influence of process parameters on the electrical conductivity of injection molded polypropylene-graphite composite products</i>
7.1. Injection molded bipolar plates of polymeric conductive composites
7.2 Materials, Equipment, and Methods
7.2.1 Materials
7.2.2 Injection molding equipment
7.2.3 Measuring methods
7.2.4 Estimate the Injection Pressure Method
7.4 Optimisation the parameters with the Taguchi method
7.4.1 Select the project and form the team
7.4.2 Plan the experiments and discussions
7.4.3 Factors

7.4.4 Levels
7.5 Results and discussions
7.5.1 TGA analysis
7.5.2 Taguchi analysis BP weight – larger-the-better
7.5.3 Taguchi analysis BP electrical conductivity – larger-the-better
7.5.4 Injection molded BP electrical resistivity
7.5.5 Injection molded BP thermal conductivity
7.5.6 PEMFC performance
7.5.7 Inorganic content influence on viscosity and injection molding pressure
7.6 Conclusions regarding the influence of process parameters on the electrical the conductivity of injection-molded products
<i>Chapter 8. Thermodynamic evaluation of polymer-carbon hybrid composites conductivity</i>
8.1. Introduction
8.2. Materials, equipment, and methods
8.2.1 Materials
8.2.2 Bipolar plate model
8.2.3 Micromanufacturing the mold surfaces
8.2.4 Injection molding equipment
8.2.5 Measuring apparatus
8.2.6 Measuring electrical resistance and resistivity
8.2.7 Evaluate the thermal conductivity
8.2.8 Evaluate PEMFC performance
8.2.9 Variation
8.2.10 Thermodynamic adapted Bueche model for electrical resistivity prediction
8.3 Results and discussion
8.3.1 Influența parametrilor de proces asupra proprietăților materialelor termoplastice compozite
8.3.2 Conductive particle dimension effect on BP electrical conductivity
8.3.3 PEMFC performance equipped with BP of C1-C4 recipes
8.4. Economic highlights
8.5. Conclusions regarding the thermodynamic analysis of the conductivity of polyethylene-carbon black-expanded graphite hybrid composites
<i>Chapter 9. Conclusions and contributions</i>
9.1 Conclusions
9.2 Contributions
Bibliography (extras)
APPENDIX A – Published works and contributions of authors
APPENDIX B – Author’s Reviews

Keywords

surface texture, additive manufacturing, non-conventional technologies, laser beam machining, molds, injection molding, conductive thermoplastics composites, bipolar plates, hydrogen fuel cells

Part I Background and Literature Review

Chapter 1. Polymer matrix composites for injection molding

Due to their superior properties to ordinary materials, composites have been used since ancient times, according to [102]:

- in MESOPOTAMIA in 3400 B.C.E., pieces of wood were cut at various angles, and plywood was made; around 1500 BCE in Egypt, clay bricks were reinforced with straw;
- 1907 - Leo Baekens perfected bakelite;
- 1935 - Corning launched the first glass fiber-reinforced polymer composites;
- 1953 - Corvette car made with fiberglass reinforced resin body [103]
- Carbon fiber was patented in 1961;
- 1979 - Dacia 500 bodywork was made of fiberglass-reinforced composites. [104]
- 1983 – The "Swatch" wristwatch had 51 polymer markers;
- In 2004, the "graphene" structure was identified and extracted
- 2000 – The Boeing 787 airplane was built with about 50% of its components made of composites.
- the 2000s – conductive polymer composite materials used to fabricate bipolar plates.

The continuous phase (matrix) can be constituted by [101]:

- metals with a higher density than alternative materials;
- ceramics and inorganic glass;
- polymers;

„**COMPOSITE** - <fiber reinforcement> solid product consisting of two or more distinct phases, including a binding material (matrix) and a particulate or fibrous material. (Example: molding material containing reinforcing fibers, particulate fillers or hollow spheres” – def. 2.182.1 SR EN ISO 472-2013 [105]. Polymers are thermoplastic, elastomeric, or thermosetting.

„**THERMOPLASTIC**, adjective, capable of being softened repeatedly by heating and hardened by cooling through a temperature range characteristic of the plastic in the softened state, of being shaped by flow repeatedly into articles by molding, extrusion or forming ” – def.2.1177 [105]

„**THERMOPLASTIC**, noun, plastic that has thermoplastic properties.” -def. 2.1178 [105] Thermoplastics are *standard* (ex. PE, PP, PS), *engineering thermoplastics* (ex. PA, PC, PC/ABS, PMMA, PBT/PET), and *high-performance thermoplastics* (ex. PPS, PSU, PEEK, PEI).

1.5.2. Conductive polymer composites

Electrical conductivity is the physical propriety of a material. Polymers are used mainly as insulators. Conductive fillers (ex., Graphite, carbon black, CNT, GNP, graphene) are added to improve the electrical conductivity of the obtained composites [124]. Percolation theory describes the behavior of a network when nodes or links are added and can be used for polymer composite conductivity prediction. Broadbent and Hammersley [125] introduced a simple "lattice percolation" model for fluid flow through a porous medium. Kirkpatrick [127] extended the theory to the three-dimensional conductance model of conducting and nonconducting materials mixtures. [146], [147].

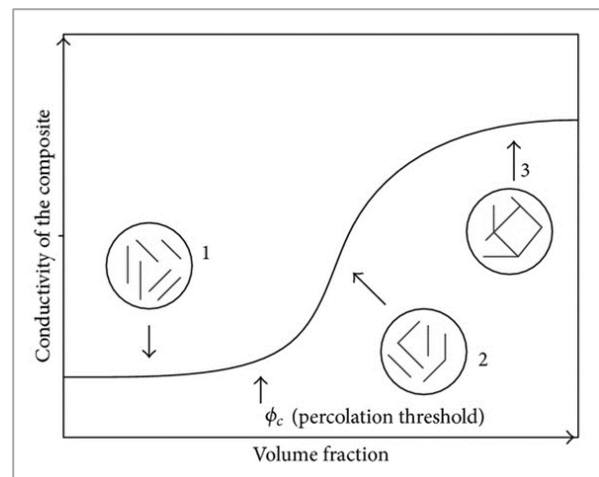


Fig. 1.5 Percolation threshold, courtesy Vargas-Bernal et al. [147]

1.7. Injection molding of thermoplastic composites

The injection molding of polymer composite products is one of the most used manufacturing methods. It is characterized by high productivity, a high degree of finishing of the part, and low costs. The initial investment in the injection mold design and manufacture recommends using this process for large production runs. EN ISO/ASTM 52900-2022 specifies that “*the shaping of materials into objects within a manufacturing process can be achieved by applying one or a combination of three basic principles:*”

- **FORMATIVE SHAPING:** “*the desired shape is obtained by applying pressure to a body of raw material*”(examples: forging, bending, casting, injection molding, compression);
- **SUBTRACTIVE SHAPING:** “*the shape of the product is acquired by selective removal of material*” (examples: milling, turning, drilling, EDM);
- **ADDITIVE SHAPING:** “*the desired shape is acquired by successive addition of material.*”

“*The objects, or parts, with acquired shapes can be combined into more complex shaped products by joining different parts in physical, chemical or mechanical operation, such as welding, soldering, adhesive, fasteners.*” [160]

ISO 427 definition 2.492: Injection Molding is a “*process of molding a material by injection under pressure from a heated cylinder through a sprue into the cavity of a closed mold.*”

ISO 427 Mold (die) definition 2.626: “*assembly of parts enclosing the space (cavity) from which the molding takes its form.*” [105] The surface texture of the mold cavities has a functional and aesthetic role. Fig. 1.11 shows a section of an injection mold showing the main components, adapted from [176] and indicating the cavity surface and the replicated surface of the molded product.

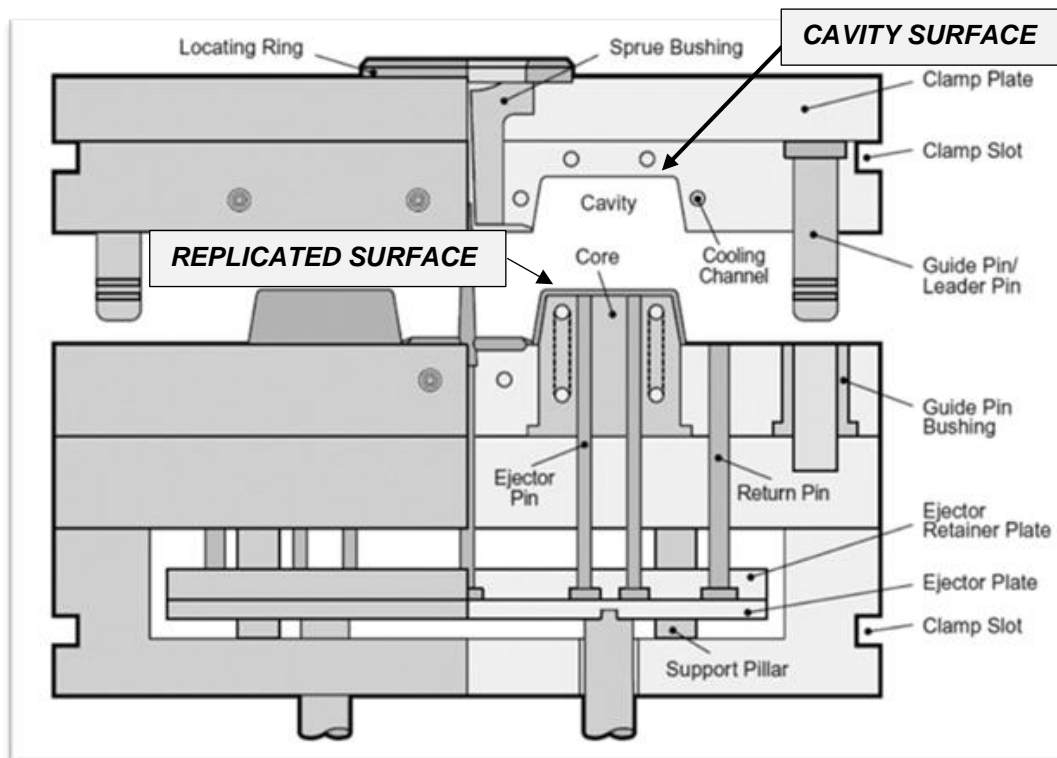
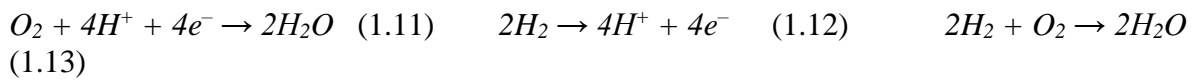


Fig. 1.11. Molds components, adapted from Bayer [176];

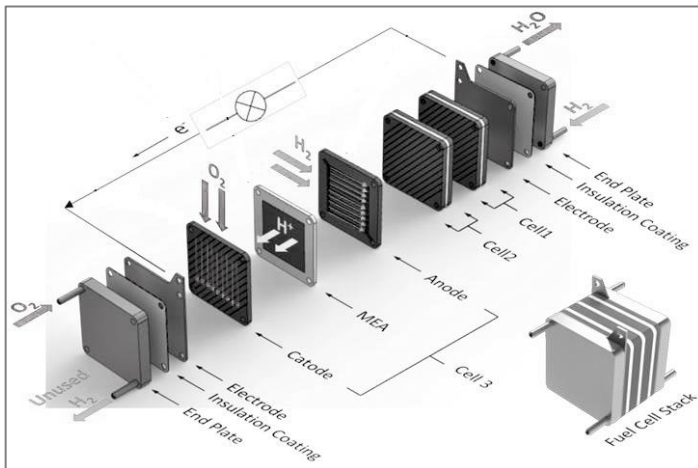
1.7.10 Applications in the energy industry: bipolar plates for fuel cells

The energy field is of prime importance to society. Decarbonizing production, recycling, and developing products and technologies based on sustainable concepts are targets of today's society. Hydrogen fuel cells have been identified as among the new renewable energy technologies needed to achieve a 60% to 80% reduction in greenhouse gases by 2050 [188].

Hydrogen fuel cells are electrochemical devices that convert hydrogen and oxygen into heat, electricity, and water. [187] The PEM fuel cell consists of a negatively charged electrode (anode), a positively charged electrode (cathode), and a proton membrane. Hydrogen is oxidized at the anode, and oxygen is reduced at the cathode. Electrons are sent in the external circuit. Protons are transported from the anode to the cathode through the proton membrane. The fuel transport in the BP's flow channels is carried out through a porous layer of electrically conductive carbon [189]. Reactions in the fuel cell are described by equation (1.11) - cathode, equation (1.12) – at the anode, and the general equation (1.13) [189], [190]:



Bipolar Boards (BP) connect several cells in series to achieve the desired power [189]. Bipolar plates are traditionally made of graphite, titanium, stainless steel, and electrically conductive composites. It must have very good electrical and thermal conductivity and must perform the following functions [189]: homogeneous distribution of gases over the entire surface of the plates; separating the combustion gas from the oxidizing gas and preventing leaks; collecting the voltage produced as a result of electrochemical reactions; the discharge of water produced as a result of the chemical reaction.



Research has been undertaken on the electrical and permeability properties, the influence of the size of the gas discharge channels in bipolar plates, and their optimization for fuel cell efficiency (Carcadea et al. [194] and [195], [196].)

Fig. 1.15 Extended fuel cell, from Chen et al. [190]

Fig. 1.18 shows a simple serpentine flow channel at the anode. Table 1.7 shows the technical specifications of the bipolar plates

Fig. 1.18 PEMFC Bipolar plate at the anode (single serpentine circuit) and cathode (parallel) [198]

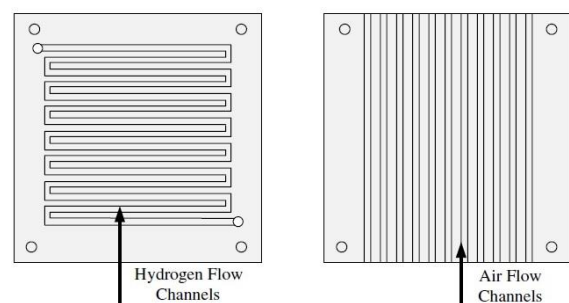


Table 1.7 Specifications Ruge și Büchi [192] and US Department of Energy – targets for bipolar plates technical parameters [197]

Specification	Units	2001 [192]	2015 Status [197]	Target 2020 [197]
Cost	\$/kW	As low	7	3
Weight	Kg/kW		<0.4	0.4
H ₂ permeability	mbar L s ⁻¹ cm ⁻²	10 ⁻⁷	0 ^{a)}	<1.3 x 10 ^{-14 a)}
Corrosion	μA/cm ²	As low	<0.1	<1
Thermal conductivity	Wm ⁻¹ K ⁻¹	20 ^{b)} , 100 ^{c)}		
Electrical conductivity	S cm ⁻¹	> 10	>100	>100
Specific Resistance	Ohm cm ²		0.006	<0.01
Flexural strength	MPa	25	>34 ^{d)}	>25 ^{d)}

a)Std cm³/(s cm² Pa) @ 80 °C, 3 atm 100% RH; b) integrated cooling circuits; c) removed heat only at edges; d) carbon plates

Chapter 2. Texturing the mold cavity surfaces

The quality of the mold cavity surfaces influences the subsequent aesthetic and functional characteristics and the extraction of the product. In this work, we directed the study, especially to the industrial manufacturing methods and the influence of the surface texture on some properties of the injection molded product. A unique surface finish, adding the specific properties of the polymer composite and its adaptation to the finishing processes, can contribute to the different behavior of the product as a whole. At the same time, the cavity surface's quality also affects the costs of the injection molded product. Brinksmeier et al. consider micromachining to include all mechanical, physical, chemical, conventional, or non-conventional methods to obtain products with micrometric precision, details, or dimensions. [201]. The structures of textured surfaces are in the micrometric domain. Usually, the texturing of the mold surfaces is obtained by manual and ultrasonic polishing, sandblasting, electrical discharge machining, or chemical etching, and nowadays, processing based on laser ablation (see def. 3.1.1 ISO 23020:2021 [206]) has become a standard technique. The product designers indicate the texture patterns, CAD or image-type files, or the models available with specialized texturing services suppliers. Texture brilliance can be mentioned according to SAE J361, a procedure for visual evaluation of the interior and exterior automotive trim.

Table 2.1 Comparison of conventional and non-conventional machining processes [202],[205]

Method	Conventional	Non-conventional
Tools	Physical Tool	It might not be physical
Wear Tool	Yes	No (or negligible)
Contact	Direct with the workpiece	No, or very low for the not physical tools
Accuracy	Lower	High accuracy and surface finish
Examples	Milling, Turning, Drilling, Boring, Grinding	Ultrasonic USM, Water Jet Abrasive, Chemical Etching, Electrical discharge machining EDM, Electron Beam Machining – EBM, Photons -LBM, Ion Beam Machining IBM

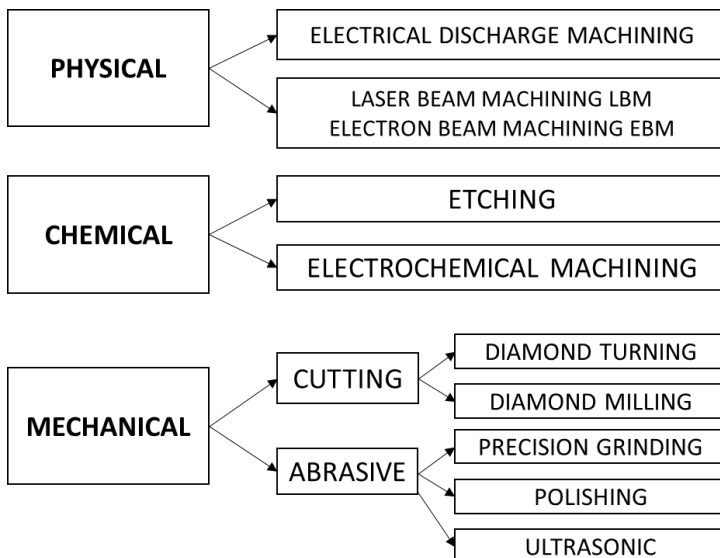


Fig. 2.1 Surface micromachining methods, adapted from Brinksmeier and Preuss [201]

Groover defines non-conventional machining as: "the material addition is removed by mechanical, thermal, electrical, chemical or combinations thereof and that does not use a cutting tool in the conventional sense." It proposes a classification of non-traditional machining processes as follows: mechanical (ultrasonic, water jet abrasive), electrochemical (electrochemical machining, electrochemical grinding, and deburring), thermal processes (electrical discharge machining EDM, electron beam machining – EBM, photons -LBM, electric arc cutting, "oxyfuel-cutting processes"), chemical (chemical etching) [202, p.628].

2.1. Geometric specification of mold cavities surfaces

Berglund et al. [216] suggested combining different approaches developed by experts in a system that describes specific surface texture parameters, according to ISO 25178 [210]. The approach to

clarify and unify the terms was confirmed by the new editions of ISO 21920-2:2021 [213] and ISO 25178-2:2021 [214]. ASRO adopted both standards in 2022.

2.1.1 Surface texture

ISO 21920-2:2021 (*Profile*) [213] cancels and replaces ISO 4287:1997, ISO 12085:1996, ISO 13565-2:1996, and ISO 13565-3:1998, which have been technically revised, and new definitions and clarifications were introduced for a correlation with ISO 25178 (*Areal*) [214]

Table 2.2 Surface texture definitions

Terms	Definition
Surface Texture	"...consists of the repetitive or random deviations from the nominal surface of an object". [202] (2011)
Surface Texture	"is a complex condition resulting from a combination of roughness (nano and micro-roughness), waviness (macro-roughness), lay and flow." [217] (2012)
Surface Texture	"is the local deviation of a surface from a perfectly flat plane." [218], (2012)
Surface Texture (Profile)	"geometrical irregularities contained in a scale-limited profile" def. 3.1.2 ISO 21920-2:2021 [213]
Surface Texture (Areal)	"geometrical irregularities contained in a scale-limited surface" (def. 3.1.2 ISO 25178-2:2021) [214]

The surface quality analysis consists of microstructural characterizations, texture and areal integrity evaluation, and relationships between manufacturing processes and the characteristics of the resulting surface [202]. Fig. 2.2 shows the surface texture schematically. Table 2.2 presents some terms and their definitions related to surface texture.

2.1.2. Geometrical specifications of surfaces

ISO (the International Organization for Standardization) developed the ISO 25178 standard [214], specifying the terms, definitions, and parameters for determining surface texture using locally applied methods. The ISO 25178 standard redefined surface texture theories *based on the principle that objects are defined in 3 dimensions in nature*. (Fig. 2.3 and Table 2.4) In this sense, specific new terms have been defined. The general concept of "scale-limited surface" was introduced, similar to the concept of "scale-limited profile" in ISO 29120 [213]. It has been established that surface textures can be isotropic or anisotropic (fig. 2.3) [217], [218], [219].

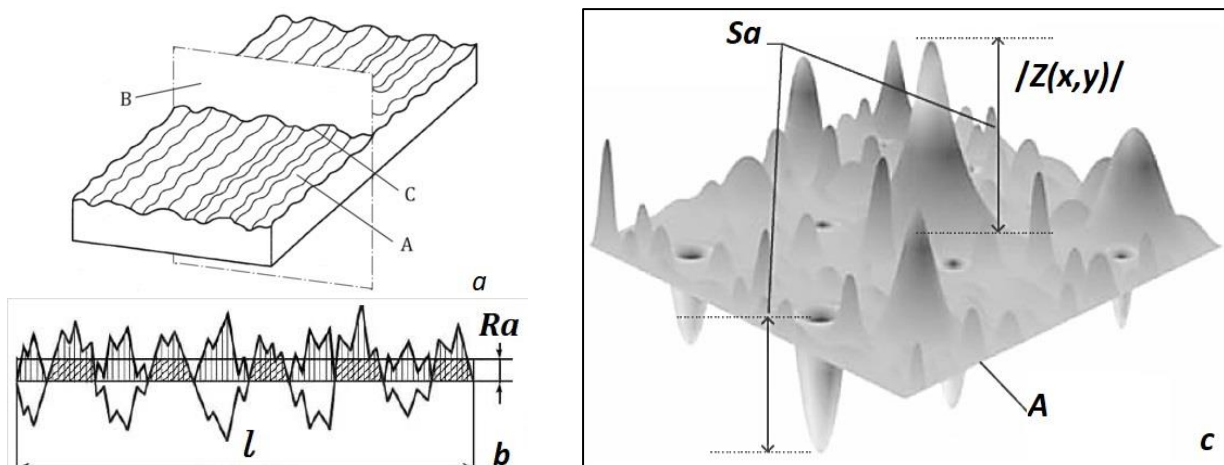


Fig. 2.3 a) A- Non-ideal surface model; B – Intersection plane; C- Profile curve (cf. ISO 21920-2 [213]); b) Ra [213] c) S_a , the arithmetical mean height of the scale limited surface) [214],[220].

Table 2.4 Definitions ISO 17450-1:2011 [221]

Term	Definition
<i>Real Surface</i>	“set of features which physically exist and separate the entire workpiece from the surrounding medium” (def. 3.1)
<i>Surface Model</i>	“model representing the set of physical limits of the virtual or the real workpiece” (def.3.2)
<i>Nominal Model</i>	“model of the perfect shape defined by the designer” (def. 3.2.1)
<i>Non-ideal surface model</i> <i>Skin model</i>	“model of the physical interface of the workpiece with its environment”(def.3.2.2)

ISO 25178 section 4.1.7 defines Sa as an extension of Ra (arithmetic mean deviation of a profile) over a surface. As an absolute value, it expresses the difference in each point's height compared to the surface's arithmetic mean. This parameter is generally used to evaluate surface roughness. It can be calculated with the formula (2.3): Fig. 2.5 shows a single example of height $Z(x,y)$, but all surface changes are evaluated in actuality:

$$Sa = \frac{1}{A} \int_A \int Z(x, y) dx dy \quad (2.1)$$

Where Sa is the arithmetic mean value of the surface height (limited to scale), $Z(x, y)$ is the height in absolute value at the limited area corresponding to the position x, y , and A is the area for which Sa is defined (Fig. 2.3c) [214].

A surface profile is defined as a "profile that results from the intersection of the real surface by a specified plane" (ISO 4287:1997, definition 3.1.4) [207]. Ra , the most used amplitude parameter, arithmetic mean deviation of the assessed profile, is defined on the roughness length and is used to evaluate the roughness of a profile [207]. The Ra arithmetic mean of the absolute ordinate values $Z(x)$ within a sampling length can be estimated with equation (2.1) according to ISO 4287 section 4.2.1:

$$Ra = \frac{1}{l} \int_0^l Z(x) d(x) \quad (2.2)$$

Where $Z(x)$ is the absolute value of the profile ordinate, and l is the length of the roughness profile. In two dimensions, the other parameters are classified according to *primary profile* (Pa) and *waviness profile* (Wa) [207].

2.1.3 Correlation Ra – Ch VDI 3400

The standard VDI 3400 – 75 *Electrical Discharge Machining (EDM), Definitions, Production, Application*, (ger. *Elektroerosive Bearbeitung; Begriffe, Verfahren, Anwendung*), is the base of indicating the grade of the surface texture, typical for mold makers. Fig. 2.6 shows a visual scale according to VDI 3400-75.

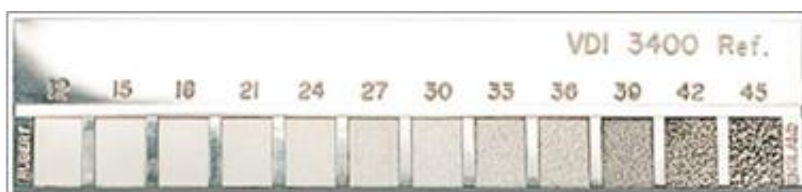


Fig. 2.6 VDI 3400 Scale [215]



Fig. 2.7 SPE/SPI a)A1 b) D3

2.1.4. Specifications SPE/SPI

The Society of Plastics Industry specifies 12 degrees of finish for the mold surfaces. Each level of finish implies a different grade of the abrasive used for texturing the surface. A surface finish comparison chart shows that each finishing level is correlated with a Ra value Fig. 2.7 shows the appearance of two surface finish samples, grades A1 and D3 [224].

2.1.5. Finishing mold cavities surfaces

Manual or ultrasonic polishing, sandblasting, *EDM*, chemical, and laser etching are commonly used surface texturing techniques. Traditionally, selective finishing of the mold cavities was done for high quality by chemical etching. Nowadays, laser texturing is preferred. The laser also executes high-precision masks for direct exposure for photochemical processing. In injection mold execution, the term surface texturing is frequently used [208], [235]. French car manufacturers use the term "*gravage chimique*" or "*grainage*" and "*grain*" for the resulting textured pattern on the surface of the mold. Brinksmeier and Preuss use the term "micromachining" for "*a machining method in which small pieces of material are removed to achieve high geometric precision that could not otherwise be achieved*" and classify the domains *nano*, *micro*, *macro* according to Table 2.6 [201].

2.2. Subtractive methods for mold cavities surface texturing

In this section, we mention subtractive technologies frequently used for the selective finishing of mold cavities: Mechanical processing (Fig. 2.12), abrasive technologies (grinding, lapping, honing, Ultrasonic Machining - *USM*), photochemical machining (or chemical texturing, photo-etching), Fig. 2.8ab [209]), Electrical Discharge Machining - *EDM*, Fig.2.9, 2.10), Electrochemical machining, laser beam machining *LBM* Fig. 2.8cd [210], Fig. 2.22, 2.23). Ion beam machining - *IBM* and Electron Beam Machining -*EBM* are mainly used in manufacturing microelectronic devices and sensors.

Table 2.6 Range of Nano, Micro si Macro Machining, Bricksmeier et al. [201]

	Nano	Micro	Macro
Surface machined	$1 \div 100.000 \mu\text{m}^2$	$1 \div 100.000 \text{mm}^2$	$1 \div 100.000 \text{cm}^2$
Volume	$10^{-3} \div 10^2 \mu\text{m}^3$	$10^{-3} \div 10^2 \text{mm}^3$	$10^{-3} \div 10^2 \text{cm}^3$
Productivity	$< 1 \mu\text{m}^3 \text{s}^{-1}$	$< 1 \text{mm}^3 \text{s}^{-1}$	$< 1 \text{cm}^3 \text{s}^{-1}$
<i>Sa</i> (equation 2.1)	$1 \div 10^2 \text{\AA}$	$1 \div 10^2 \text{nm}$	$10^{-1} \div 10^2 \mu\text{m}$

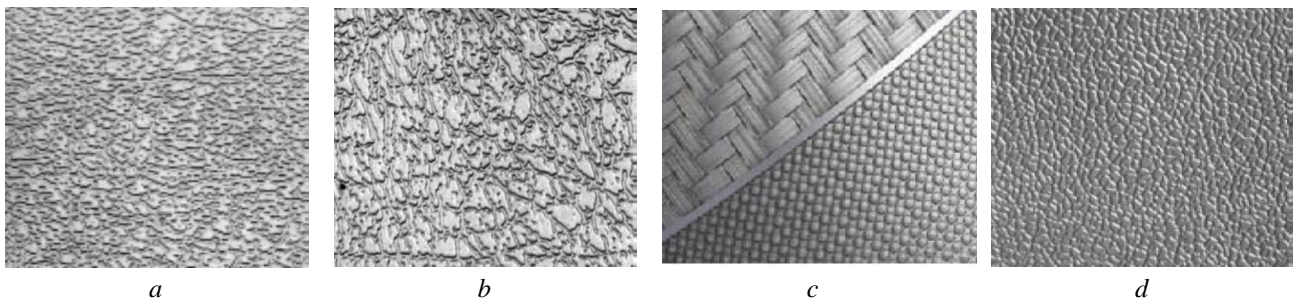


Fig. 2.8 Surface textured samples a) b) chemical etching [225]; laser texturing c) [209] d) [210]

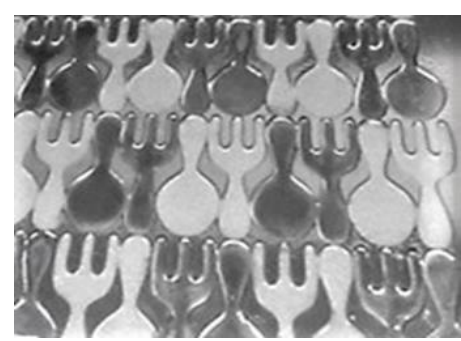
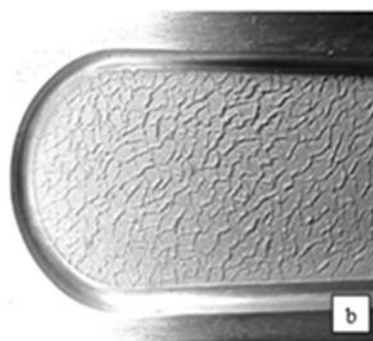
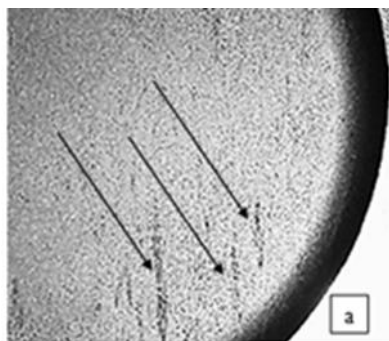


Fig. 2.9 a) Cavity surface machined in DIN 1.2312 steel by milling and finishing by EDM VDI 3400 #30 with a copper electrode, showing defects (vertical marks) due to high sulfur content; b) EDM #24 "skin" like texture on aluminum alloy EN 7075 machined with EDM VDI 3400 #24 using copper electrode (courtesy LS Inteh)

Fig. 2.10 Selective EDM VDI 3400 #30 and #09, respectively, on DIN 1.2085 steel at 30-33 HRC (courtesy of LS Inteh SRL).

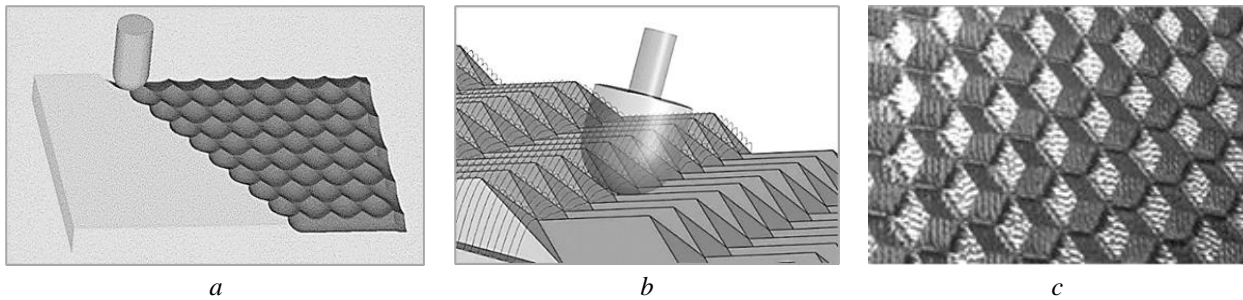


Fig. 2.12. Examples of surface generation by micromachining. a) micro-milling simulation with a "parallel" strategy; b) the parallel tool traces; c) surface appearance of the micro-milled surface cavity on DIN 1.2311 steel at 30-33 HRC (image kindly provided by LS Inteh SRL).

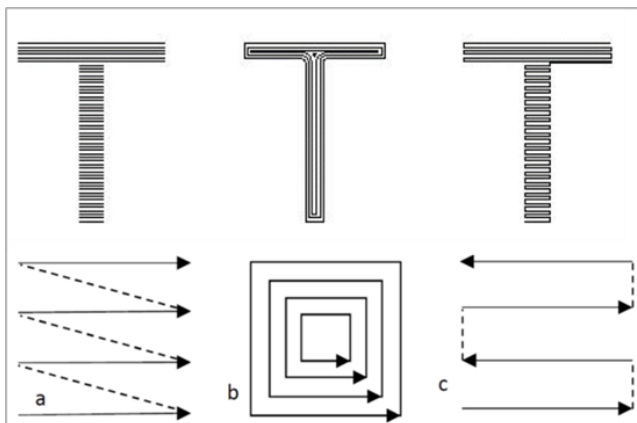


Fig.2.22. Laser beam strategies are a) unidirectional, b) "ring" like, and c) bidirectional [245].

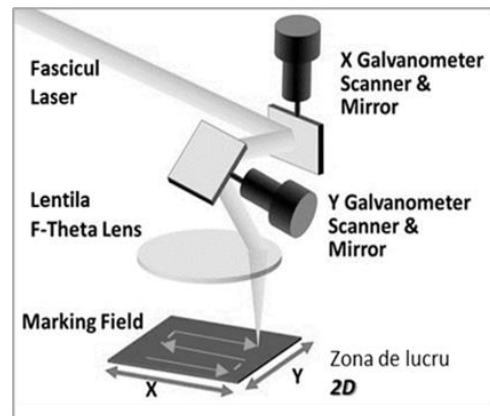


Fig. 2.23 Working principle of a fiber laser for 2D marking/engraving/texturing

2.3 Additive manufacturing methods of mold metal cavities

SR EN ISO/ASTM 52900-2022 defines "Additive modeling: the desired shape is obtained by successively adding material." The standard classifies additive manufacturing (AM) methods into seven classes [207]. For the additive modeling of metals, we mention the classes: POWDER BED FUSION (PBF), DIRECTED ENERGY DEPOSITION (DED), ADDITION OF LAYERS (SHEET LAMINATION - SHL), classes shown in Fig. 2.27, BINDER JETTING (BJT, see Chapter 5.)

2.8 Micromachining research directions

Research activities are directed to technologies such as electrochemical micro texturing (*ECM_{tex}*) with or without a mask, "electrochemical spark" micromachining (*EC_{SMM}*) as a hybrid *ECM* + *EDM* process [204], "Micro chiseling" – diamond machining of molds for optical components on a nickel substrate [201], processing in the micro or nanometric field (*micro-EDM*, *micro-ECM*), ultrasonic-assisted *EDM* (*EDM+US*) [280]; laser-assisted machining (*LAM*) [281],[282], lithography, electroplating, and molding (LIGA, ger., Lithographie, Galvanoformung, Abformung) [283], Fabrication of biomimetic surfaces- *PDMS*, and Embedded Elastomeric Stamping (*PEES*).

An extensive research project *eVerest*, funded by the German Federal Ministry of Education and Research, was dedicated to the development of a system for processing and designing 3D surface texture of large injection molds, with objectives such as validation of precision laser structuring technologies (DMG MORI), developing one ps ultrashort pulsed laser (AMPHOS), CAD techniques for texture evaluation (VOLKSWAGEN), development of a dynamic laser focus positioning system (SCANLAB), investigation of precision of ultrashort pulse duration laser ablation (FRAUNHOFER ILT), achieving Z-axis focus change with deformable mirrors (MUNSTER UNIVERSITY OF APPLIED SCIENCES), software solutions for generating textures for large components (VISUAL COMPUTING INSTITUTE & RWTH AACHEN UNIVERSITY [289].

Chapter 3. Conclusions regarding the research of surface texturing methods for the injection molding of thermoplastic composite products

3.1.1. Properties of thermoplastic composites

A thermoplastic composite material consists of a matrix of a meltable polymer to which reinforcement/filler materials are added in various forms and specific volume/mass percentages.

- Reinforcing/filling materials used for polymeric materials do not chemically interact substantially with the matrix but can take over various loads during mechanical stress.
- In order to obtain good electrical resistivity, a graphite particle content of over 70% is required in the case of products made from polymer matrix composites.
- The inorganic content influences the flow behavior during injection by increasing the viscosity of the composite, which requires higher processing temperature and pressure values.

3.1.2. Testing methods of conductive thermoplastic composite materials

Most global research has been directed toward the characterization of composites obtained by laboratory methods using reinforcement materials such as *GNPs*, *CNTs*, or *graphene*. The conductivity prediction models considered the particles' orientation, shape and size, and percolation theory.

As a result, the activity in this doctoral thesis focused on developing a less explored injection molding technology using raw materials available on the market at affordable prices (polypropylene, polyethylene, graphite, expanded graphite, carbon black).

3.2 Conclusions regarding surface quality, processing, and generation methods

Some researchers believe that a combination of surface description systems is helpful. Thus, the discussion of the quality of the surfaces of the product shaped by injection molding carried out in direct connection with the functional role allows a correct evaluation, which does not depend on the validity of the method and the measurement deviations of the equipment. We adopted such an approach throughout the tests and analyses of the doctoral thesis. The quality of the surfaces influences the electrical contact resistance.

3.3 Micromanufacturing mold surfaces technologies

Manufacturing processes are based on physical, chemical, or mechanical methods. They use or combine three principles: *FORMATIVE SHAPING* (e.g., injection molding of the product), *SUBTRACTIVE SHAPING* (conventional and non-conventional methods), and *ADDITIVE SHAPING* (e.g., for metals, *DED*, *PBF*, *SHL*, or *BJT* methods). The thermoplastic product designers describe the *Surface Texturing* patterns, and the mold makers manufacture accordingly. *Surface structuring* describes the effect of a type of processing that affects the material's structure at a superficial layer level. *Micromachining* refers to productivity under one cube millimeter per second, a roughness *Sa* from one to one-hundred nanometers, and the surface topography details in the micrometric range. In the same approach, *microinjection* can indicate a detail or precision of the molded product in the micrometric range. The term *micro profiling* can be appropriate when the texture results from the "traces" left by the tool on the programmed travel paths or extruded products.

Part II. Contributions

Chapter 4. Objectives, research methodology, and structure of the doctoral thesis, published papers

4.1. Surface texturing methods for thermoplastic composites injection molding

Actual research directions are related to the following:

- Theoretical and experimental study of micromanufacturing;
- Theoretical and experimental research dedicated to laser ablation microprocessing; laser focus positioning systems, CAD systems for texture description;
- Correlation models between process parameters and the quality of surfaces;
- Texture of the surfaces of the molds with an aesthetic or functional role;
- Analysis of the influence of the texture of the mold surfaces on the properties of the product;
- Studies regarding the correlation of process parameters with the properties of the molded product;
- Optimization of processes and the integration of methods in the industry.
- Development of conductive polymer composites for injection molding PEMFC bipolar plates.

4.2. The objectives

Therefore, we choose the *main objective*:

Advanced technologies for texturing the mold cavity surfaces and their replication in the injection molding of thermoplastic composites, with an application in the energy field – bipolar plates for hydrogen fuel cells.

The *specific objectives* were set as follows:

- Experimental study of micro-milling, photochemical machining *PCM, LBM, EDM, AM (BJT class)*;
- Development of a sequential system for complex processing by micro-milling and laser texturing;
- Effects of surface quality and process parameters on physical product properties;
- Correlations between the process parameters and the quality of the laser-textured surfaces;
- Development of new economic thermoplastic conductive composites based on standard materials
- Development of the injection molding technology of PEMFC bipolar plates.

4.3. Directions

- *Non-conventional (EDM, PCM) and advanced manufacturing methods (LBM, AM)*;
- *Conductive thermoplastic composite materials for components of energy production devices.*

4.4. Research methodology

Background and literature review are presented in the first part of this thesis, and the second part is dedicated to the primary and specific objectives. Chapter 5 follows the "*scientific method*" for analyzing advanced manufacturing technologies (examples of their industrial validation and implementation were included in sections 5.5 and 6.7), and Chapters 6, 7, and 8 with a "*bottom-up*" approach specific to industrial engineering. The methodology involved studying surface topography by optical and electronic scanning microscopy, measuring roughness, and testing the physical characteristics of thermoplastic composites. We also mention the literature overview, design of the experiments, and optimization through statistical methods.

The works completed during the doctoral studies are presented in the Bibliography section [401-409] and APPENDIX A, and the reviews in APPENDIX B. (Daniel Serban, Web of Science Researcher ID: AAE-6269-2021, ORCID ID: <https://orcid.org/0000-0002-8361-212X>)

Chapter 5. Advanced technologies for texturing cavity surfaces and their replication by injection molding

5.2 Experiments

5.2.1 Model

We designed a “family” mold for a product consisting of two plates with dimensions of 50 mm x 50 mm x 2.5 mm; on one face, four impressions were photochemically machined (abbreviated *PCM 1, 2, 3, 4*), and four impressions textured by laser beam machining (*LBM 1, 2, 3, 4*). On the opposite face were designed four impressions to be electrical discharge machined (*EDM 18, 24, 30, 36*), two by milling (*MIL1, 2*), and two inserts made by additive technologies of the class *BJT*, metal jet binding (abbreviated *MBJT1, MBJT2*). We added a specimen *1BA* ISO 527 [142], an 80 mm x 10 mm x 4 mm *IZOD* specimen conforming to ISO 178 [143], and a disc 30 mm in diameter and 3 mm thick. (3D model in Fig. 5.3, the mold in Fig. 5.4, “S” – position of cavity pressure sensor)

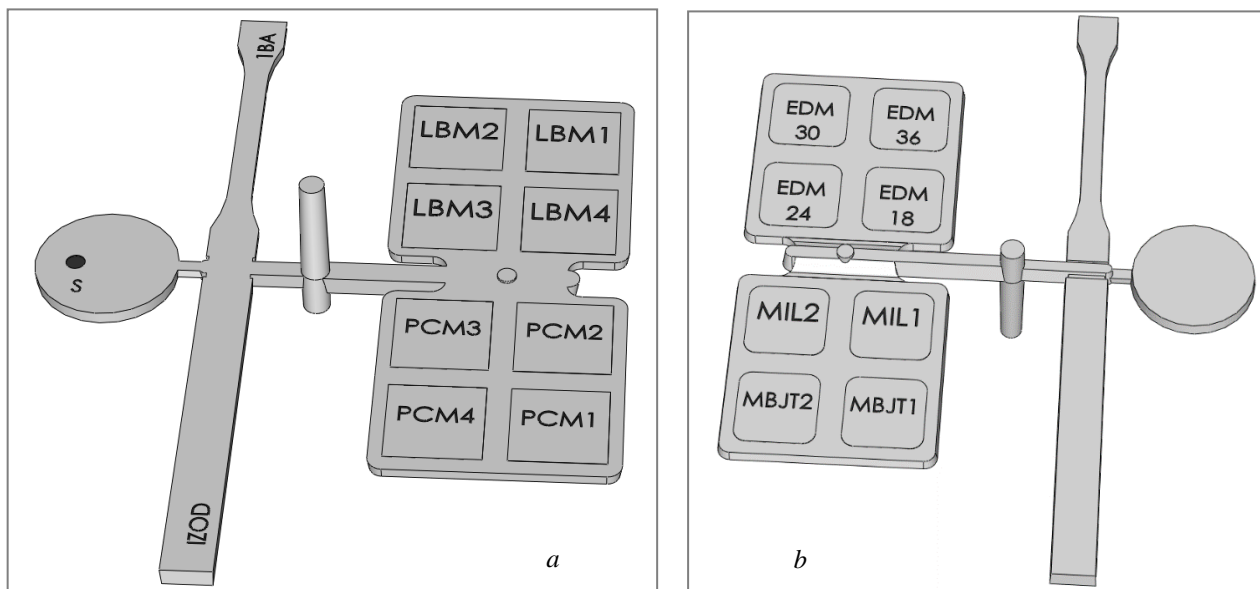


Fig. 5.3 The 3D Model, components, and textured impressions

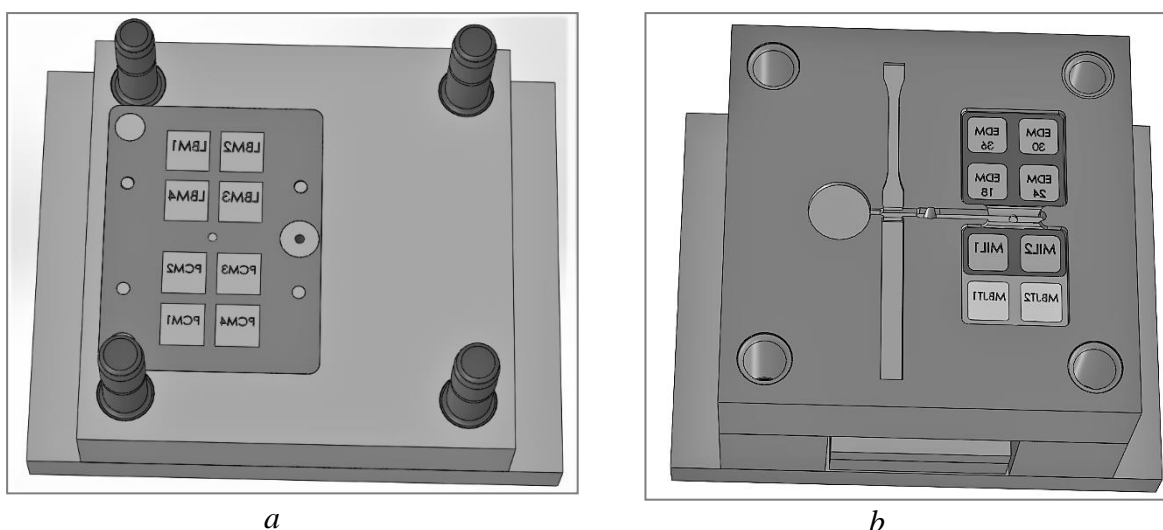


Fig. 5.4 The mold a) injection side with laser (*LBM*) and photochemical machined (*PCM*) impressions; b) ejection side with the *EDM*, milled (*MIL*) impressions, and *MBJT* inserts

5.2.2 Conductive thermoplastic composites

We developed recipes C6 and C7 (Table 5.2) of conductive composite materials by adding expanded graphite SIGRATHERM® GFG 1200 SGL from Carbon GmbH (Table 5.3) and graphite RINGSORFF® R8500 powder (Table 5.4) to C5 - a masterbatch polypropylene matrix and carbon black filler with a particle size of 20 nm from PLASTIKA KRITIS SA Greece (table 5.1)

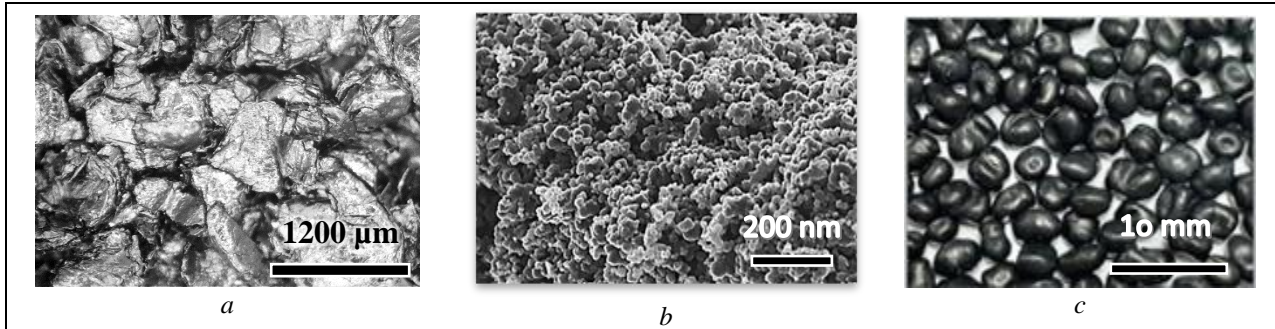


Fig. 5.5 a) SIGRATHERM® GFG 1200 expanded graphite flakes; b) carbon black SEM image, courtesy [501]; c) Capture granules PP942P

Table 5.1 Composite PP – CB PP942P Specifications

Components	Material	Proprieties	Method
Matrix	PP-homopolymer	MFR=25 g/10 min@190°C	ISO 1133-1
Filler	Carbon black	Particle Dimension = 20÷25 nm	
Inorganic content	-	40,00 ± 1.20	OEE-8.2.4-01-06
Composite	PP - CB	MFR=6,4 g/10 min 10kg@230°C(*)	ISO 1133-1

Information supplied Plastika Kritis SA, Greece, exception (*) evaluated at Cardinal Srl, București

Table 5.2. Composites recipes developed on a matrix of PP-CB (Fig. 5.1 a, c)

Composite	Granule PP942P		Flakes* PP942P		Filler 2 EG GFG 1200	Filler 3 Powder GR
	Matrix PP	Filler 1 CB d 20 nm	Matrix PP	Filler 1 CB d 20 nm		
C5	30%	20%	30%	20%	-	-
C6	28,5%	19%	28,5%	19%	5%	-
C7	27%	18%	27%	18%	5%	5%
PP flakes*	-	-	100%	-	-	-

(*) ISO 472-2013 definition 2.1691 „flake – plate-like regrind.”

Table 5.3 Proprieties of expanded graphite EG SIGRATHERM® GFG 1200 SGL Carbon GmbH

Proprieties/(Norm)	Units	GFG 1200
Dimension D ₅₀ (DIN51938)	μm	1200
Powder density (DIN 51705)	g/l	200
Carbon content (DIN 51903; 800°C; 20h)	%	≥95
Humidity (DIN51901; 110°C; 8h)	%	≤5

Table 5.4 Proprieties of graphite GR RINGSORFF® R8500

Proprieties	Units	Graphite R8500
Density	g/cm ³	1.77
Average granulation	μm	10
Flexural strength	MPa	50
Electrical resistivity	μΩm	14
Thermal conductivity	Wm ⁻¹ K ⁻¹	80

5.2.3. Mold cavities materials

On a Euro standard mold base, we machined the pockets for the inserts on the plates made of steel DIN 1.2312 at 30-33 HRC. The additive method *BJT* was used for manufacturing the inserts in steel SS 316 L (DIN 1.4404). The inserts for evaluating subtractive processes were alloyed steel hardened and tempered to 27HRC—chemical composition evaluation in Tables 5.5 and 5.6.

5.2.5 Injection molding equipment

We performed the injection molding experiments on the Battenfeld Plus 35 machine, Austria (350 kN clamping force, equipped with an injection unit with a 30 mm diameter screw, 60 cm³ capacity, at a maximum pressure of 110 Mpa. The mold was electrically heated, and cavity pressure was evaluated with DME P4000 equipment. The parameters are shown in Table 5.18.

5.2.6 Metallography analyses equipment

The microstructures of metallic or non-metallic surfaces were analyzed in the LAMET laboratory from UPB and kindly provided by Prof. Dr. Eng. Ionelia Voiculescu.

5.3 Results and discussions

5.3.1 Chemical composition results

The metallographic analysis of the surfaces of the metal molds was carried out at the LAMET laboratory, UPB; the EDS chemical composition results are presented in Tables 5.5 and 5.6, and the spectrum of the elements present in the alloys are shown in Fig. 5.6 and 5.7.

Table 5.5 Low alloy steel plates chemical composition (EDS method)

Element	C	Si	Mn	Fe	Co
%wt	0,62	0,89	0,59	97,34	0,56

Table 5.6 EDS chemical composition of BJT inserts (DIN 1.4404)

Element	Al	Si	Mo	Cr	Mn	Fe	Ni
%wt	4,66	1,19	1,60	18,05	1,43	63,07	10,01

5.3.2 Photochemical machining method

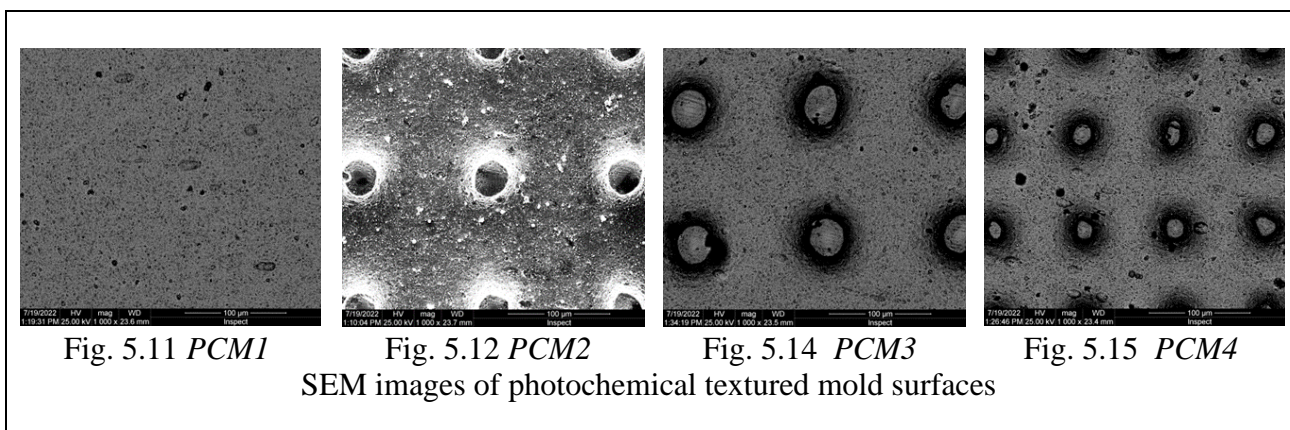
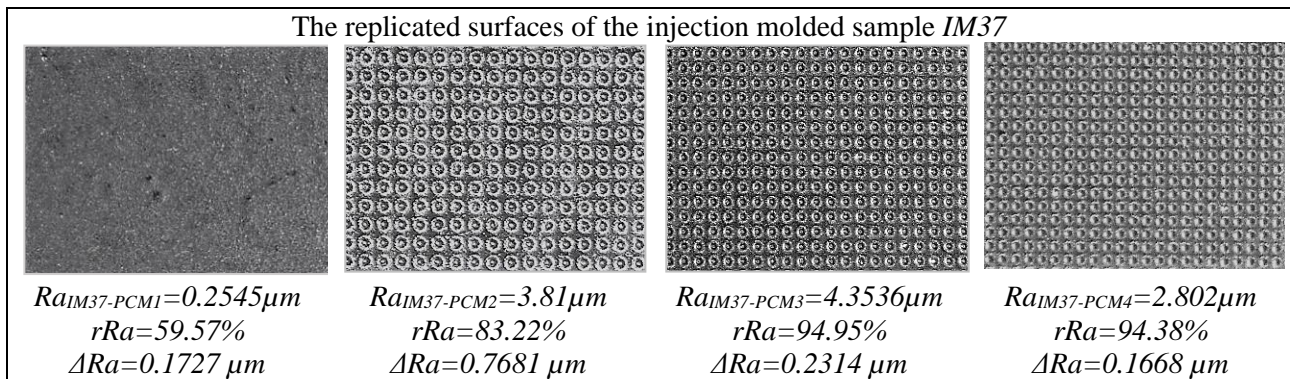
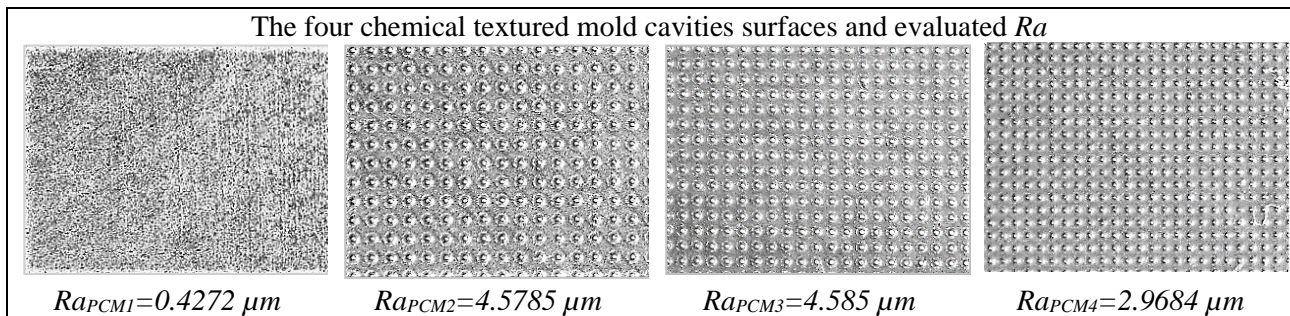
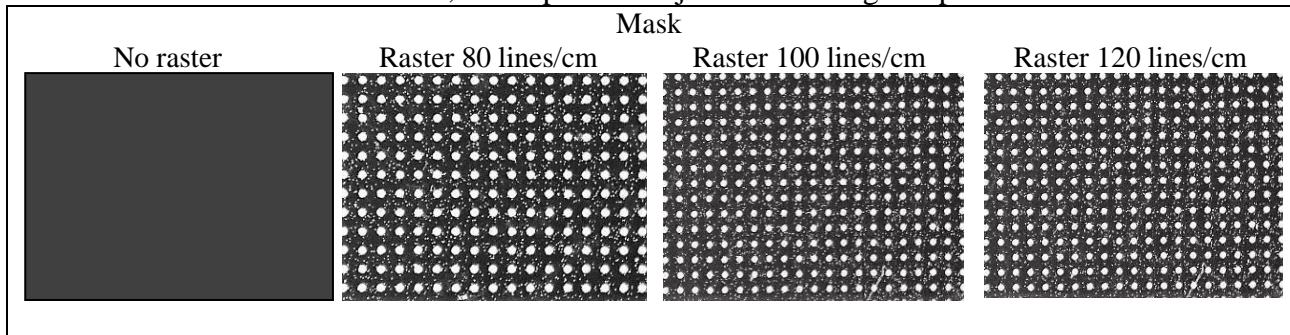
The photochemical machining (chemical etching, exposure method with mask) was subcontracted to EDG Bucharest. Four patterns were chosen: without raster, with raster 80 lines/cm - 90% filling, 100 lines/cm - 90% filling, and 120 lines/cm - 90% filling. Table 5.7 shows details of the masks, chemical textured mold surfaces, and the molded product replicated surfaces, details of an area of 2 x 1.5 square millimeters- corresponding magnification 20:1. The roughness Ra is indicated as Ra_{PCM_i} , respectively $Ra_{IM37-PCM_i}$. It represents the arithmetic mean of five measurements in one direction, respectively, and five measurements in a second perpendicular direction for each analyzed surface (Fig. 5.8). The surface roughness was measured with the Vogel apparatus, Germany.

For all processes analyzed, the replication rate rRa was evaluated as a ratio of Ra measured on the injection molded sample no. 37 (*IM37*) and the corresponding Ra of the mold cavity surface, with formula (5.1a) and respectively the difference ΔRa , with formula (5.1b):

$$rRa = Ra_{IM37}/Ra_{mold} [\%] \quad (5.1a)$$

$$\Delta Ra = Ra_{mold} - Ra_{IM37} [\mu m] \quad (5.1b)$$

Table 5.7 Details areas of 2 mm x 1.5 mm surfaces (scale 20:1) of masks, photochemical textured cavities surfaces, and replicated injection molding sample nr. 37

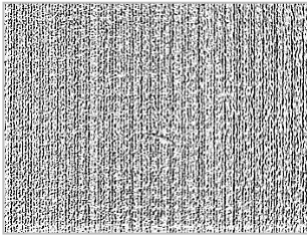
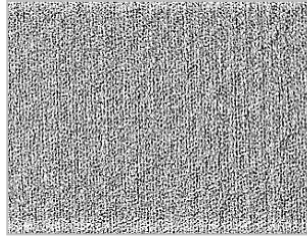

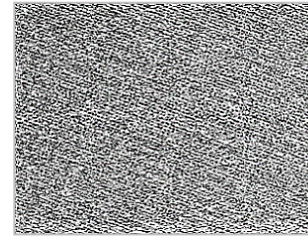

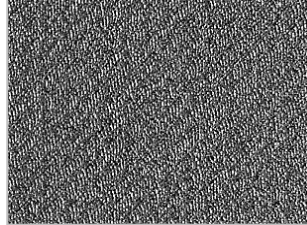
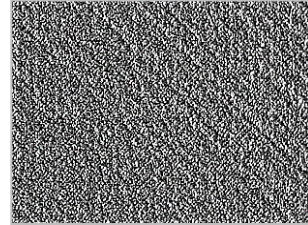
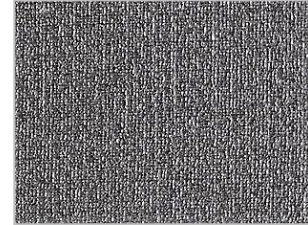


Reasonable replication rates resulted for the chemical texturing $PCM3$ and $PCM4$, a reduced rate for the sample $PCM1$, in good agreement with the roughness values recorded on the surface obtained by additive method BJT . In contrast, all other samples, $PCM2$, $PCM3$, and $PCM4$, recorded replication values of over 83% (see Table 5.7 and Table 5.17). The scanning electron microscopy observed that the chemical etching produced a texture with regular geometry, with the lowest roughness recorded for sample $PCM1$. (see Fig. 5.11-5.15)

5.3.3 Laser texturing

The laser processing was performed on the same alloy steel plates used for the photochemical processing (Table 5.5), using a *Q-Switch* fiber laser with a wavelength of 1064 nm, maximum power of 20W, and pulse duration of 120÷150ns and 0.66 mJ maximum energy of the pulse.

Table 5.9 LBM parameters, details of textured cavities, and replicated injection molding surfaces

<i>LBM 1</i>	<i>LBM 2</i>	<i>LBM 3</i>	<i>LBM 4</i>
P = 60% [of 20W] V = 500 [mm/s] Frequency = 20 [kHz]	P = 60% [of 20W] V = 800 [mm/s] Frequency = 30 [kHz]	P = 90% [of 20W] V = 500 [mm/s] Frequency = 30 [kHz]	P = 90% [of 20W] V = 800 [mm/s] Frequency = 20 [kHz]
Details of LBM areas 2 mm x 1.5 mm			
<i>LBM 1</i>	<i>LBM 2</i>	<i>LBM 3</i>	<i>LBM 4</i>
			
$Ra_{LBM1} = 1.058 \mu\text{m}$	$Ra_{LBM2} = 0.876 \mu\text{m}$	$Ra_{LBM3} = 1.142 \mu\text{m}$	$Ra_{LBM4} = 0.977 \mu\text{m}$
Details of replicated injection molded sample nr. 37 areas 2 mm x 1.5 mm			
			
$Ra_{IM37-LBM1} = 0.8167 \mu\text{m}$ $rRa = 77.2\%$ $\Delta = 0.241 \mu\text{m}$	$Ra_{IM37-LBM2} = 0.586 \mu\text{m}$ $rRa = 66.8\%$ $\Delta = 0.291 \mu\text{m}$	$Ra_{IM37-LBM3} = 0.750 \mu\text{m}$ $rRa = 65.7\%$ $\Delta = 0.392 \mu\text{m}$	$Ra_{IM37-LBM4} = 0.517 \mu\text{m}$ $rRa = 52.96\%$ $\Delta = 0.459 \mu\text{m}$

Four sets of laser beam processing parameters were chosen, *LBM1..4*; Table 5.9 presents the parameters' values, the representative images of the laser-textured surfaces, and the replicated injection molding ones. Processing control was carried out with the help of the *EZCAD2* application, on vector paths, with double hatching (according to Fig. 2.22a, Chapter 2)

Table 5.10 Laser parameters and corresponding Ra evaluation

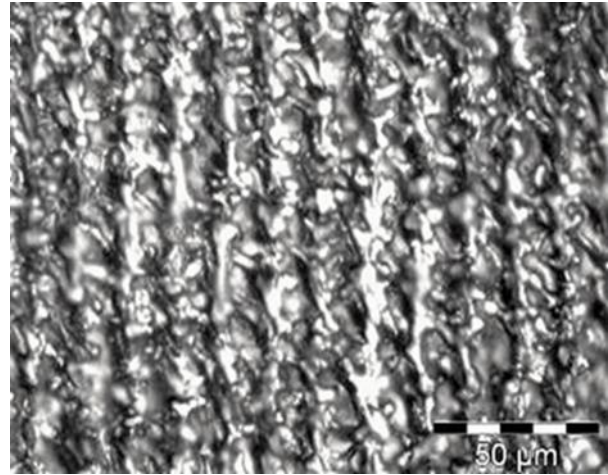
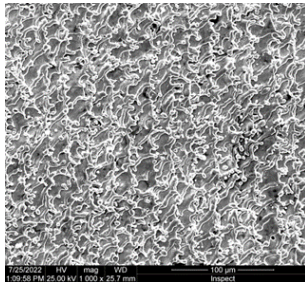
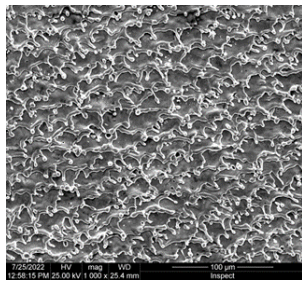
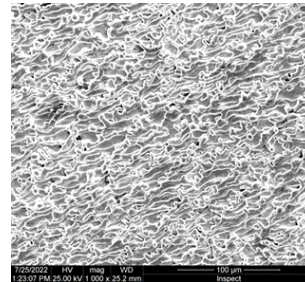
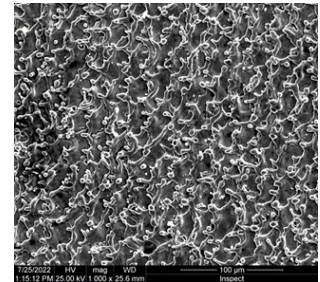
LBM No.	Power	Speed [mm/s]	Frequency [kHz]	$(y_i) = (Ra_{D1} + Ra_{D2})/2$ [μm]					MSD	SN Ratio
				1	2	3	4	5		
1	60	500	20	1.0	1.012	1.038	1.089	1.062	0.89563548	0.4787
2	60	800	30	0.8	0.892	0.876	0.948	0.847	1.31323478	-1.1834
3	90	500	30	1.1	1.138	1.124	1.128	1.160	0.76718060	1.1510
4	90	800	20	0.9	1.006	0.993	0.987	0.992	1.05312131	-0.2248

An L4 orthogonal array was chosen for the experiments, three factors, power, speed, and frequency, with two levels (Table 5.10). Taguchi *larger-the-better* and ANOVA (table 5.12) analyses revealed the dominant effect of beam travel speed and beam power on roughness Ra – interpreted here as productivity, larger Ra – associated with higher material removal rate.

Table 5.12 ANOVA

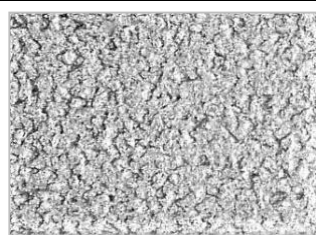
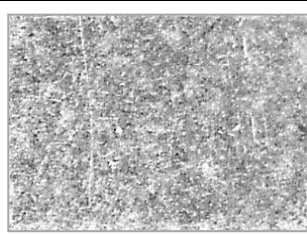
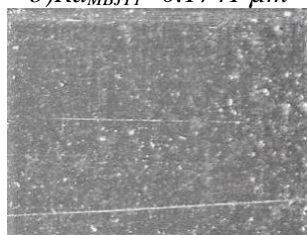
Factors	Levels		Freedom Degrees	Standard Deviation	Variation MS	Factor Effect
	1	2				
Power	-0.3524	0.4631	2	0.6650	0.3325	22.2
Speed	0.8149	-0.7041	2	2.3072	1.1536	77.1
Frecvency	0.1270	-0.0162	2	0.02050	0.01025	0.7

We presented in the thesis chapter 2.2.7 the experiments carried out by Piccolo et al. [255] of injection molding replication of laser textured mold surfaces (wavelength 1030 μm , pulse duration (ultrashort) 310 fs, pulse energy 2.51 μJ , speed 1500 mm/s, frequency 250 kHz). Although the values of the temperatures T_m 90 $^\circ\text{C}$ and T_m 120 $^\circ\text{C}$ used in the mentioned experiments were far outside the range recommended for PP (30÷50 $^\circ\text{C}$), we observed the values of roughness samples PP/ T_m 90 $^\circ\text{C}$ [255], close to those of the replicate *LBM1* *IM37* samples injection molded in our experiment PP flakes/ T_m 45 $^\circ\text{C}$. (Fig. 5.16)

Fig. 5.16 Microscope image of *LBM1* surfaceFig. 5.17 *LBM1*Fig. 5.18 *LBM2*.Fig. 5.19 *LBM3*Fig. 5.20 *LBM4*

SEM images of laser-textured mold surfaces

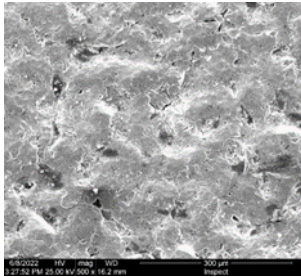
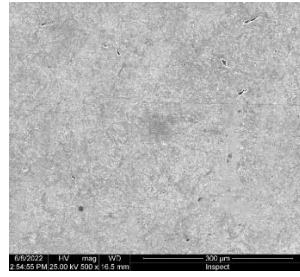
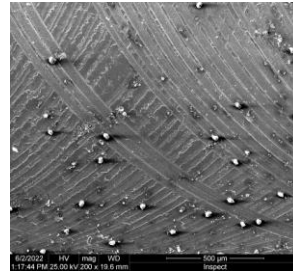
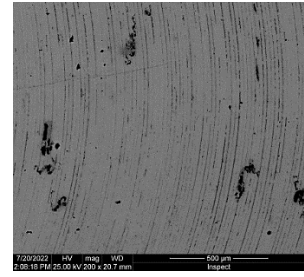
5.3.4 Additive method *BJT*

a) $Ra_{MBJT2} = 4.530 \mu\text{m}$ b) $Ra_{MBJT1} = 0.1741 \mu\text{m}$ c) $Ra_{IM37-MBJT2} = 4.148 \mu\text{m}$
 $rRa = 91.5\%$
 $\Delta = 0.381 \mu\text{m}$ d) $Ra_{IM37-MBJT1} = 0.15 \mu\text{m}$
 $rRa = 86.16\%$
 $\Delta = 0.0241 \mu\text{m}$

Two inserts were made with the *BINDER JETTING*, *BJT* method. (ISO 52900 [257]) We use the abbreviation *MBJT* (Metal-*BJT*). The additive process consisted of depositing a layer of 316L metal powder, followed by its leveling, and then "*printing*" by jetting the binder selectively, consolidating with thermal energy, and repeating the deposition procedure layer by layer until the object was completed. After removing the excess powder, the "*printed*" product was consolidated by sintering in special furnaces at temperatures corresponding to the base materials.

Fig. 5.21 Details of mold *MBJT* areas 2mmx1.5mm and replication rate a) *MBJT2*; b) *MBJT1*; c) *IM37-MBJT2*; d) *IM37-MBJT1*

Company Materialize, Belgium, fabricated *BJT* method the inserts with our 3D models (step files). We evaluated the inserts in our experiments. Fig. 5.21, 5.22, and 5.23 show the *MBJT1* surface texture (Ra 0.17 μm) and *MBJT2* rough surface (Ra 4.5 μm).

Fig. 5.22 *MBJT2*Fig. 5.23 *MBJT1*Fig. 5.25 *MIL1*Fig. 5.26 *MIL2*SEM Images of *MBJT* and Milled (*MIL*) impressions

5.3.5 Milling

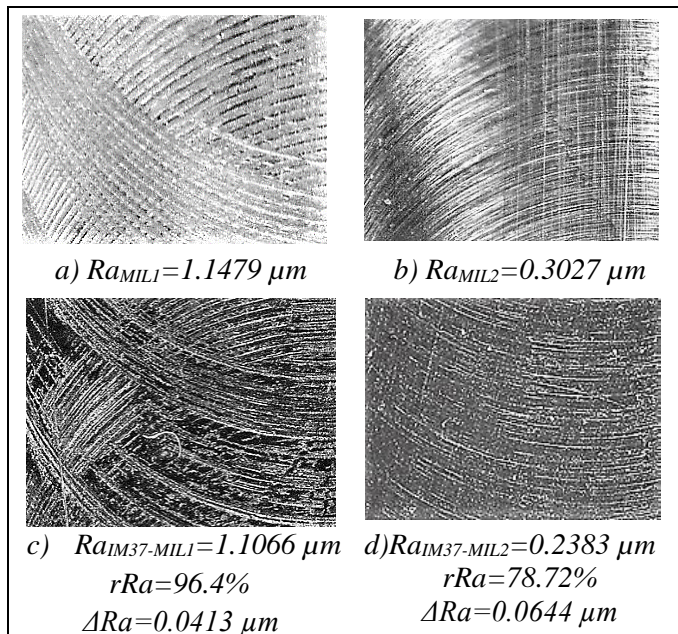


Fig. 5.25 (SEM) and Fig. 5.24a (detail of 2 mm x 1.5 mm) show the impression of *MIL1* face milled with a five millimeter TiAlN coated carbide tool with a speed of 7200 min^{-1} , cutting depth of 0.01 mm and a feed of 500 mm/min. Fig. 5.24c presents the replicated injection molded surface. Fig. 5.26 (SEM) and Fig. 5.24b show the *MIL2* impression face milled with a speed of 10,000 min^{-1} and 200 mm/min feed. Fig. 5.24d shows the corresponding molded surface. The Ra results confirmed the anticipated superior finishing of the surface machined at a higher speed and lower feed.

Fig. 5.24 Details of areas of 2 mm x 1.5 mm
a) *MIL1* b) *MIL2* c) *IM37-MIL1* d) *IM37-MIL2*

Composite shrinkage, texture detail topography, and complex (plastic and elastic) deformation during stylus method measurement can explain the replication rate $rRa=78.72\%$ for *MIL2* ($Ra=0.3027$ μm) compared to the rate $rRa=96.4\%$ for *MIL1*.

5.3.6 Electrical discharge machining EDM

Table 5.14 EDM parameters and *Charmilles* surface quality prediction

Set parameters code <i>E</i>	<i>M</i>	<i>V</i> [V]	<i>P</i> [A]	<i>A</i> [μs]	Finishing CH no.*	<i>Ra</i> [μm] predicted
363	1	+160	16	50	CH 33	4,5
303	1	+200	6	50	CH 31	3,2
243	1	+200	4	3,2	CH 24	1,62
183	4	-200	1	3,2	CH 18	0,8

(*as indicated by machine constructor Roboform 100 - Charmilles Technologies

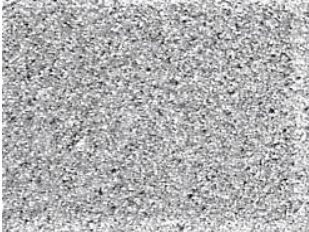
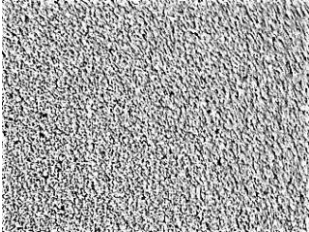
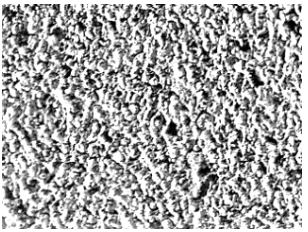
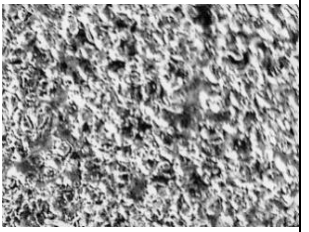
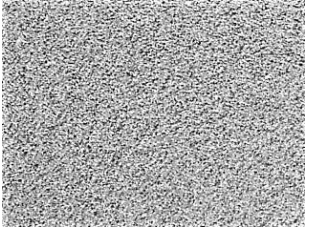
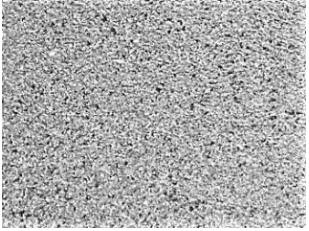
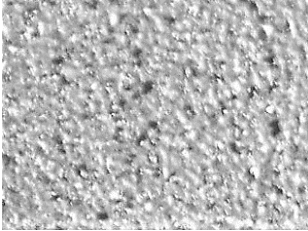
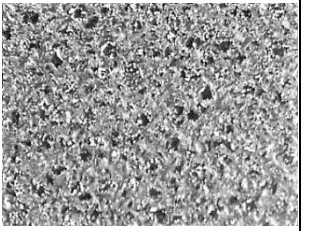
M- mode; V- Voltage [V]; P - Current [A]; A- discharge pulse [μs]; Ra [μm].

Table 5.15 show detailed images and the replication rate. Four impressions, each of about 19 mm x 19 mm, were electrical discharge machining with "predefined" parameters that predict the

roughness Ra 4.5, Ra 3.15, Ra 1.6, and Ra 0.8. Charmilles recommends a tolerance of two CH units, evaluated as follows::

$$CH\ No = 20 \log(10\ Ra) \tag{5.5} [509]$$

Table 5.15 Details areas of 2 mm x 1.5 mm EDM textured and replicated $IM37$

EDM textured cavities surfaces			
<i>EDM18</i>	<i>EDM24</i>	<i>EDM30</i>	<i>EDM36</i>
			
$Ra_{EDM18} = 0.6772\ \mu m$	$Ra_{EDM24} = 1.4432\ \mu m$	$Ra_{EDM30} = 3.0735\ \mu m$	$Ra_{EDM36} = 4.192\ \mu m$
Replicated surfaces of injection molding sample nr. 37			
			
$Ra_{IM37-EDM18} = 0.4116\ \mu m$ $rRa = 60.78\%$ $\Delta = 0.2446\ \mu m$	$Ra_{IM37-EDM24} = 1.16\ \mu m$ $rRa = 80.38\%$ $\Delta = 0.2932\ \mu m$	$Ra_{IM37-EDM30} = 2.969\ \mu m$ $rRa = 96.6\%$ $\Delta = 0.1043\ \mu m$	$Ra_{IM37-EDM36} = 3.7359\ \mu m$ $rRa = 89.12\%$ $\Delta = 0.4623\ \mu m$

Experiments observed a good replication rate for $EDM30$ ($rRa=96.60\%$) and $EDM36$ ($rRa=89.12\%$), while $EDM18$ ($rRa=60.78\%$) and $EDM24$ ($rRa=80.38\%$) indicated lower replication rates and a similar behavior influenced by the geometric texture dimension. (Table 5.15). Tables 5.14 and 5.15 indicate lower experimental Ra values than those predicted. The finer granulation of the graphite used to build the electrode can explain the phenomena.

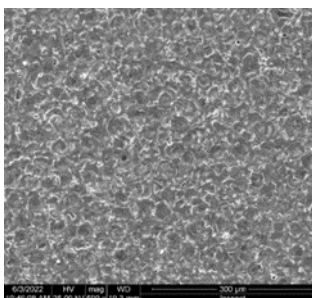


Fig. 5.33 $EDM18$

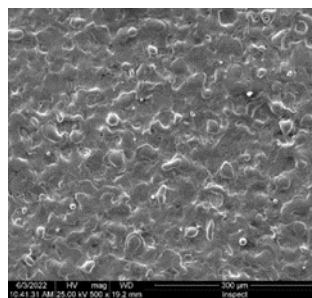


Fig. 5.34 $EDM24$

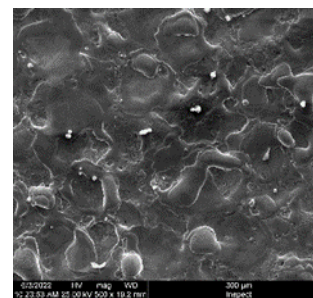


Fig. 5.35 $EDM30$

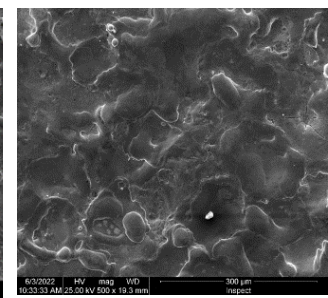
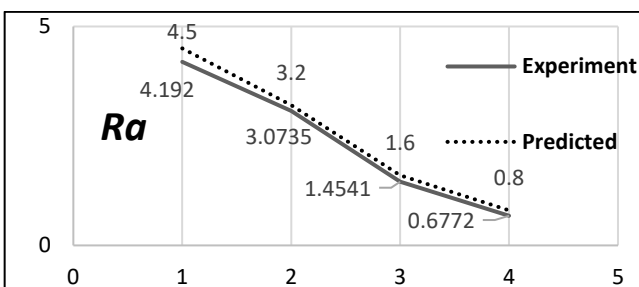


Fig.5.36 $EDM36$

SEM Images of EDM textured surfaces



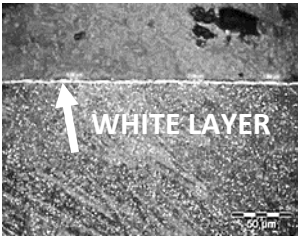
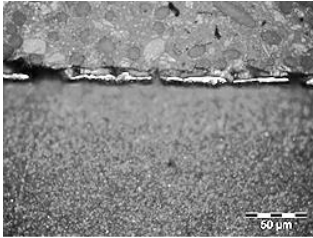
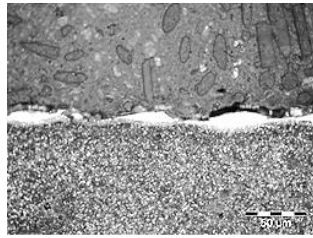
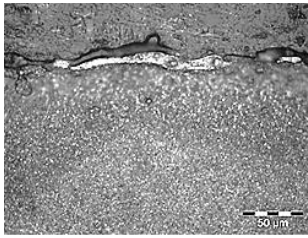
We noted close predicted and estimated surface roughness values (fig. 5.30). Our EDM experiments confirm the results of previous research, namely the important influence of current intensity on productivity and the degree of surface finish.

Fig. 5.30 Ra experimental and predicted.

5.3.7 Microhardness analysis of the EDM layer

The microhardness was evaluated with the Shimadzu HMV 2T device from the LAMET laboratory for an indentation force of 980.7mN applied for 10 seconds. The measurement conditions were: ambient temperature of 28°C and humidity of 40%.

Table 5.16 Microhardness HV0,1 of EDM layers

<i>P18 – EDM18</i>	<i>P24 – EDM24</i>	<i>P30- EDM30</i>	<i>P36 – EDM36</i>
272	347	300	293
			

The hardness of the base material recorded very close values for the four analyzed samples, differences being identified only in the "white" layer (see SEM Images of the sections in Table 5.16), where phase transformations occurred due to rapid cooling during the EDM process. The hardness value was maximum for sample P24 (347 HV0.1) and minimum for sample P18 (272 HV0.1). "White" layer hardness decreased for samples P30 and P36 compared to sample P24. Samples P30 and P36 observed dispersion of the results, the melted layer being discontinuous and inhomogeneous. Results confirm the higher microhardness of the white layer.

5.3.8 Injection molded surfaces replication

Analyzing the replication rate, we observed the following:

- Cavity Pressure and temperature can vary during the filling and packing phases, depending on the distance relative to the gate (Fig. 5.31 and 5.1). However, the replication rate rRa for the position-matched pairs (*LBM-EDM30*), (*LBM4-EDM24*), (*PCMI-MBJT1*), and (*LBM2-EDM36*) did not confirm such an influence.

Table 5.17 Ra , Ra IM37, Replication rate rRa , ΔRa , as placed into the mold

Face <i>a</i> (fig.5.3)	<i>LBM1</i>	<i>LBM4</i>	<i>PCM2</i>	<i>PCMI</i>	<i>LBM2</i>	<i>LBM3</i>	<i>PCM3</i>	<i>PCM4</i>
Ra [μm]	1.0579	0.9767	4.5785	0.4272	0.876	1.142	4.585	2.9684
Ra IM37 [μm]	0.8167	0.5173	3.81	0.2545	0.586	0.75	4.3536	2.802
rRa	77.20%	52.96%	83.22%	59.57%	66.80%	65.70%	94.95%	94.38%
ΔRa	0.2412	0.4594	0.7681	0.1727	0.291	0.392	0.2314	0.1688
	↓	↓	↓	↓	↓	↓	↓	↓
Face <i>b</i> (fig.5.3)	<i>EDM 30</i>	<i>EDM 24</i>	<i>MIL2</i>	<i>MBJT 1</i>	<i>EDM36</i>	<i>EDM18</i>	<i>MIL1</i>	<i>MBJT2</i>
Ra [μm]	3.0735	1.4432	0.3027	0.1741	4.192	0.6772	1.1479	4.53
Ra IM37 [μm]	2.969	1.16	0.2383	0.15	3.7359	0.4116	1.1066	4.148
rRa	96.60%	80.38%	78.72%	86.16%	89.12%	60.78%	96.40%	91.57%
ΔRa	0.1043	0.2932	0.0644	0.0241	0.4623	0.246	0.0413	0.381

- A tendency for better replication was found with increasing Ra value. From the analysis of the SEM images, we noted the similarity of the perception of the details related to laser processing *LBM3* or *LBM1* – microscopic image 500x (Fig.5.16) with those made by Piccolo et al. (Fig. 2.25a) [255] 24000x SEM image. However, our experiments indicate a detailed size of 10 μm , i.e., ten times larger than the Piccolo experiments [255]. Our experiments

recorded better laser machining replication rates for the same mold temperature range and holding pressure. The results indicate a correlation between the size of the detail of the mold surface topography and its replication (Fig. 5.37, for the same r , $\alpha 1 > \alpha 2$ results $h1 < h2$). The impressions $F2$ vs $F1$, $EDM18$ vs $EDM30$, and $EDM36$. (Table 5.17) confirm the statement.

- c) The evaluation method can influence the results. In the case of probe equipment, its radius and pressing force can lead to combined plastic and elastic deformations of micro-irregularities, especially in the case of polymeric materials with high plasticity.

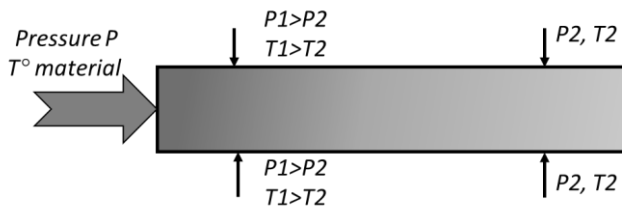


Fig. 5.36 Cavity pressures and temperatures

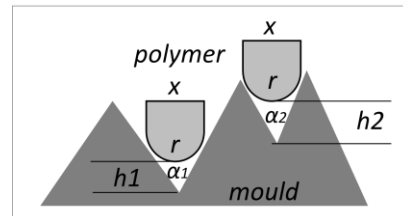


Fig. 5.37 Detail dimension replication

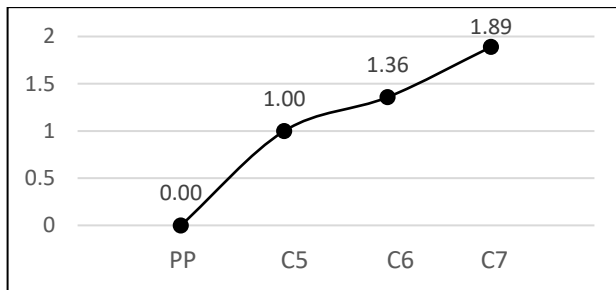


Fig. 5.38 Relative electrical conductivity

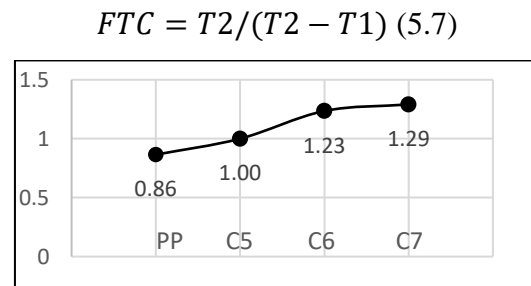


Fig. 5.41 Thermal conductivity factor

Table 5.18 Composites specifications, process parameters, and proprieties

Composite	C5	C6	C7	PP “Flakes”
Sample *	0÷8	19÷30	31÷36	37÷42
Matrix PP [%]	60%	57%	54%	100%
Filler 1 – CB [%]	40%	38%	36%	-
Filler 2 – EG [%]	-	5%	5%	-
Filler 3 – GR [%]	-	-	5%	-
Injection pressure [MPa]	87	65	65	55
Injection speed [cm ³ /s]	50	50	50	50
Holding pressure [MPa]	44	44	44	44
Holding time [s]	8.5	8.5	8.5	8.5
Cavity pressure [MPa]	23.9	26.1	27.3	12.53
Material temperature (set at the nozzle) [°C]	240	220	220	190
Cavity temperature [°C]	45	46	48	45
Cooling time [s]	60	60	60	60
Weight [g]	24.41	26.39	27.14	19.17
Melt flow index MFR ISO 1133 [g/10 min] **	6.4 g/10 min 10kg @230°C			28.4 g/10 min 2.16kg @230°C
Relative electrical conductivity ($\sigma_{C5=1}$)	1	1.3577	1.889	-
Electrical conductivity (four-point method)[S/cm]	1.081	1.468	2.043	-
Thermal conductivity factor ($FTC_{C5=1}$)	1	1.235	1.2905	0.8645

(*) data referring sample nr. 37 - IM37 (**) Measurements at Cardinal Srl

5.4 Conclusions on injection mold surfaces finishing

Laser beam micromachining has become a standard technology, and texturing of injection mold cavity surfaces is an accessible, economical method that offers new possibilities for product design and fabrication. **Photochemical machining** is suitable for fabricating precision details but with limited depth and is still a successful method for mold texturing. For laser and chemical texturing, patterns are usually indicated as image-type files (*JPEG, BMP*). **Electrical discharge machining**

EDM is a standard method in the mold and die-making industry for surface finishing. The designer can describe the cavity surface *EDM* finish and manufacture following VDI 3400 [215]. Due to technological progress, conventional and high-speed **milling** offers the advantage of high surface finishing and good productivity. The machining paths for cavities and *EDM* electrodes are calculated on the surfaces of three dimension CAD models. **Additive manufacturing methods** are becoming popular in prototyping and fabrication at reasonable costs of mold components. The inserts MBJT1 and MBJT2 ($19 \times 19 \times 1.5 \text{ mm}^3$, stainless steel 316L) used in our experiments cost 11 euros/piece. Additive methods use *STL* or *OBJ* extension-type files (which describe only the surface geometry of a three-dimensional object) exported from CAD applications. Laser scanning and photogrammetric methods can also obtain three-dimensional additive manufacturing models. The texturing process influences surface replication in injection molding. The size of the topography detail depends on the texturing method and process parameters. The influence of the shrinkage of the injection molded product on the replication of the mold surfaces is relatively low; for example, for polypropylene, we could consider it on areal to be 2.89% (1.7% on the Z axis to which we add the effect of the shrinkage of 1.7% at the same evaluation length of Ra).

5.5 Validation of mold surface manufacturing technologies

This section presents examples of industrial integration of engraving by milling, LBM, and *EDM* for micromachining or texturing performed by the author during the doctoral studies. Injection molding experiments presented in [401] confirmed the application domains for each technology. Fig. 5.42 shows the 290 mm x 120 mm surface of a hot-weld plate of a "blister" CNC engraved by micro-milling with a single-tooth tool, radius 0.1 mm, and 45° at the top, a "parallel" strategy.

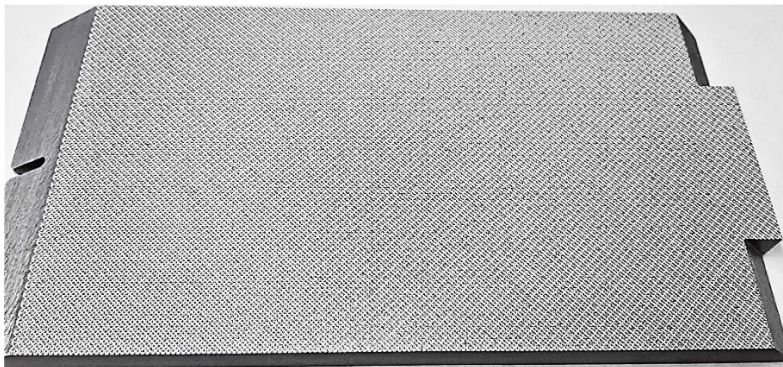


Fig. 5.42 Engraved welding plate, Aluminum EN 6068, courtesy LS INTEH srl

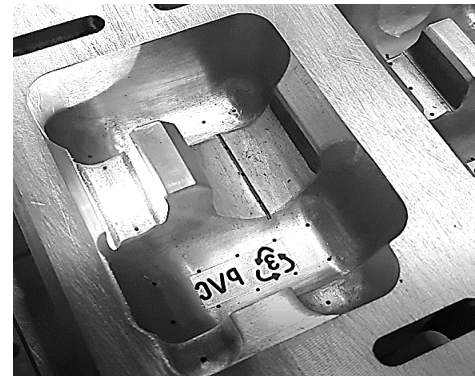


Fig. 5.43 LBM, engraving, drilling, "milling"

The engraving of the recycling signs of a thermoforming tool for the medical industry was laser beam machined using an image-type file. The strengthening ribs of $0.6 \times 0.6 \times 25$ and drilling $\text{Ø}0.5 \text{ mm}$ on a depth of 0.8 mm for vacuum access were machined on vector paths (the laser beam moving on the vectors resulted from hatching a rectangle of 0.6×25 , respectively, a circle of $\text{Ø}0.5$).

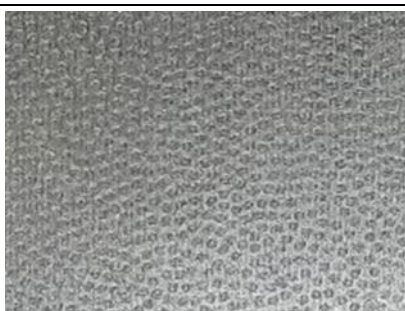


Fig. 5.44 Laser texturing, steel DIN 1.2311

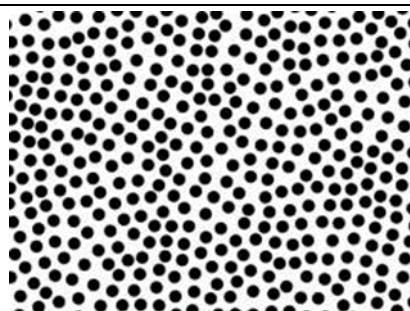


Fig. 5.45 The pattern, JPEG file

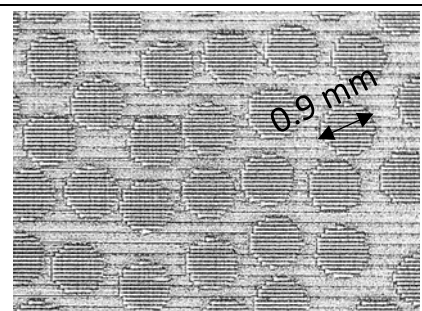


Fig. 5.46 Texture detail

Fig. 5.44 shows the surfaces of an injection mold made of DIN 1.2311 steel at 30-33 HRC, textured in 2D) with the 20W fiber laser LBM1 parameters (detail - see Fig. 5.46) with a strategy according to Fig. 2.22 and 2.23 – Chapter 2. The surface to be textured was processed by CNC milling and then prepared by manual polishing, gradually, with abrasive paper grit 180 to grit 600. Then, the surface was uniform laser-textured. The final pattern was applied by laser scanning the image *JPEG* file (Fig. 5.45) with a "dithering" method over a depth of 50 μm .



Fig. 5.47 EDM texturing VDI 3400 #22, courtesy LS INTEH srl.

Fig. 5.47 shows the cavity surfaces of an injection mold processed by EDM grade VDI3400#22 in steel DIN 1.2714 at 40-42 HRC. The author of the thesis performed the EDM on a Charmilles Roboform 100 machine with a 64A generator with a graphite electrode manufactured by CNC milling and manually polished with 1000-grit sandpaper.

Chapter 6. Development of sequential milling – laser beam machining system

6.2 Description of sequential milling – LBM system adapted to a machining center

In 2019, we first evaluated the complex sequential processing system, micro milling + laser processing. In the new technology developed by the author and shown in Table 6.1, only the laser beam was generated in continuous mode as a circle hatched with a step of hundredths of a millimeter (control with the *EZCAD2* application). The movements of the laser beam on paths were calculated on the model surface and were driven by the NC controller of the machining center. On existing dedicated equipment, the galvanometer controls the laser beam; positioning of the workpiece, including focusing 3 to 5 axes CNC controlled.

Table. 6.1 Description of sequential milling – LBM system adapted to a machining center

Equipment	Specifications	System layout
Vertical machining center	Curse x= 1000 mm, y=700 mm, z=700 mm Sistem absolut de masurare directa Controler: SELCA 3045P (for CNC milling and LBM paths)	
Ceramic bears electrical motor	24.000 min^{-1} , Air-cooled	
Fiber Laser	<i>Q-Switched fiber laser 20-watt</i> <i>Galvanometer Scanner Head</i> Controler: PC / software EZCAD2	

6.4. 2019 MM+LBM Experiments, Results, and Discussion

The complex system was built on a 3-axis vertical machining center, to which a 20 W *Q-Switch* fiber laser was added using a fixture adapted to the main spindle's SK40 taper (as described in Table 6.1) Fig. 6.1).

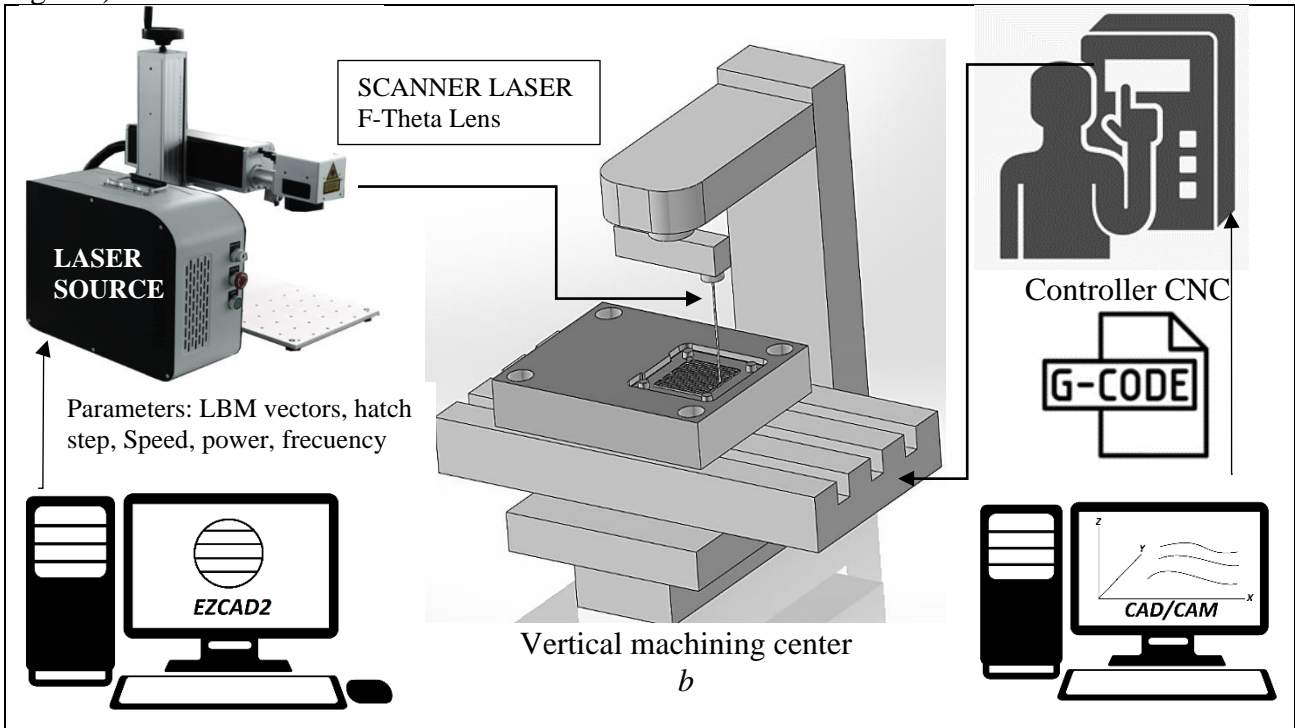

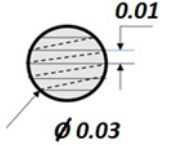
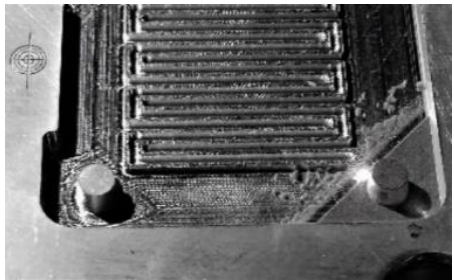


Fig. 6.1 Laser scanning head adapted to machining center Z axes

The novelty consisted of the machining with the laser beam describing a micro-tool on CNC vertical machining center-controlled paths (see Table 6.2 and Fig. 6.2c). In contrast to existing methods, the laser worked by replacing the physical cutting tool on paths generated with a parallel-type milling strategy and numerically controlled.

Table 6.2 Experiments *MM+LBM 2019* – extras positioning, milling, laser

Operation	Tools/Parameters	Controller/Program	Image during machining
Poziționare	Comparator 3D	SELCA 3045P	
Micro milling	Pocket strategy, ø0.8mm flat end mill, speed=22.000 ⁻¹ , feed = 400 mm/min	SELCA 3045P ISO 6983 (G-Code)	
LBM	Parallel strategy, 45° steps of 0.01mm, Power=18 Watt Frequency = 30Hz	SELCA 3045P ISO 6983 (G-Code)  PC-EZCAD2 laser beam ø0.03mm	

The EN7075 aluminum alloy mold cavity was micro-machined on the sequential system: rough milling, micro-milling, and laser processing (Table 6.2).

6.4.1. Influence of process parameters on surface roughness

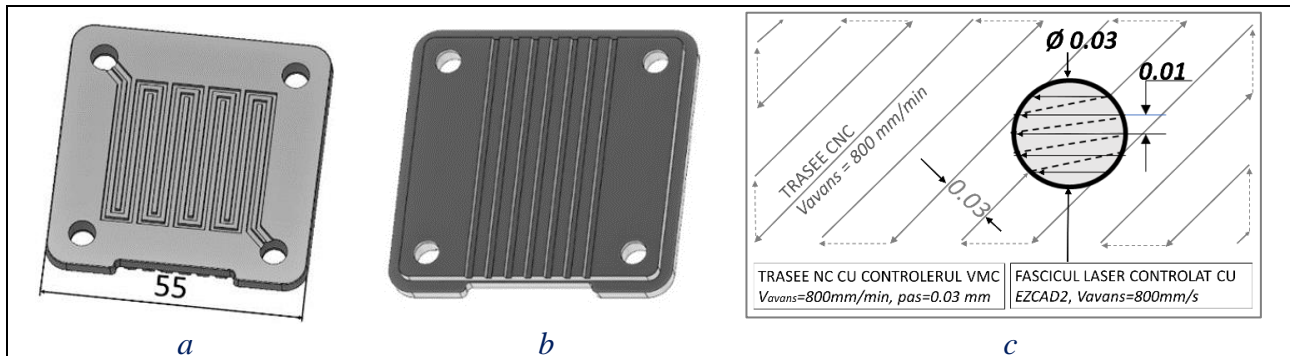


Fig. 6.2 Bipolar plate model made of conductive polymer composite 55 x 55 - 4 mm, a) anode b) cathode c) diagram of moving the laser beam replacing the physical tool on NC paths

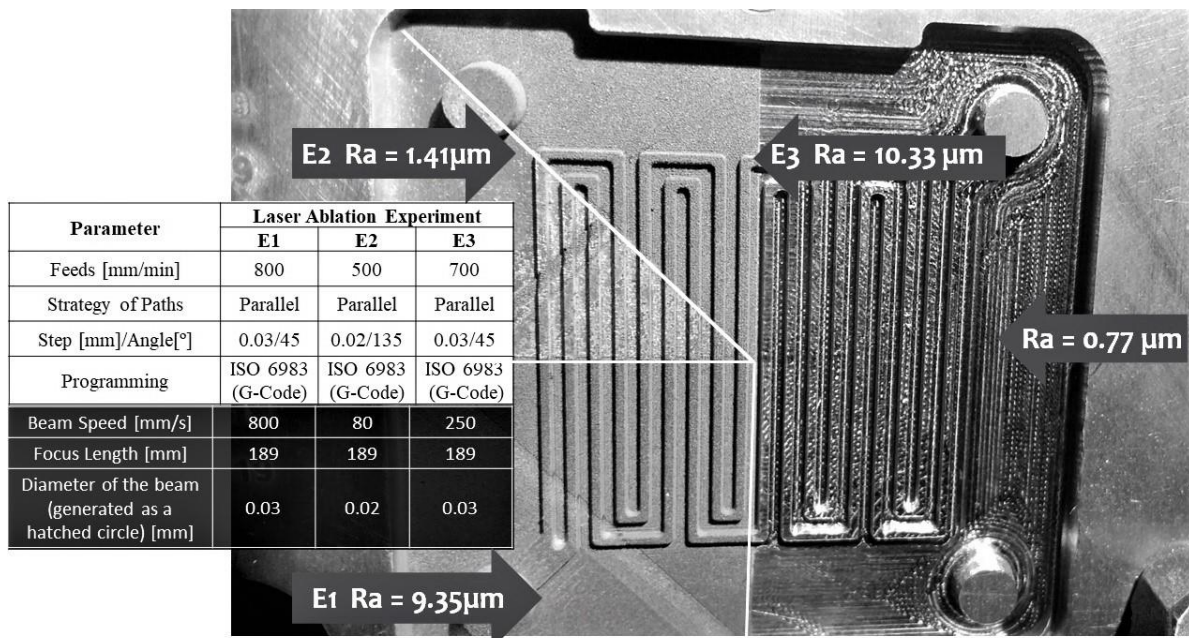


Fig. 6.3. Milled and laser textured surfaces roughness [404]

The injection molding experiments were performed on an Arburg K-221-75-350, with a reciprocating screw of 30 mm diameter developing a clamping force of 350 kN and a maximum injection pressure of 110 MPa. The cavity pressure was measured with a DME 4000 Controller and a pressure sensor DME 405 C. The roughness evaluation was performed at ICSI Vâlcea on the samples in PP87GR, and Fig. 6.3 shows the R_a values of the mold surfaces processed by micro milling and LBM with $E1$, $E2$, and $E3$ parameters. [406] We can notice the influence of the combination of laser beam scanning speed on the surface roughness.

6.4.2 Evaluation of injection molded bipolar plates in the fuel cell assembly

This section presents the results obtained with the injection molded bipolar plates in the PP87GR thermoplastic composite with polypropylene matrix and 87% graphite content (see Fig. 4.1a) assembled in a five-cell PEM fuel cell and tested as a charger for the battery of a mobile phone. The first tests of the injection molded bipolar plates of the conductive thermoplastic composite were carried out in a fuel cell stack (purchased from Fuel Cell Store, USA, see Fig. 6.4) in which we

replaced the existing CM-BP with the IM-BP of our experiments. Hydrogen and oxygen were supplied from electrolysis. Part of the results was presented at the Modtech 2020 Conference and published in [407].

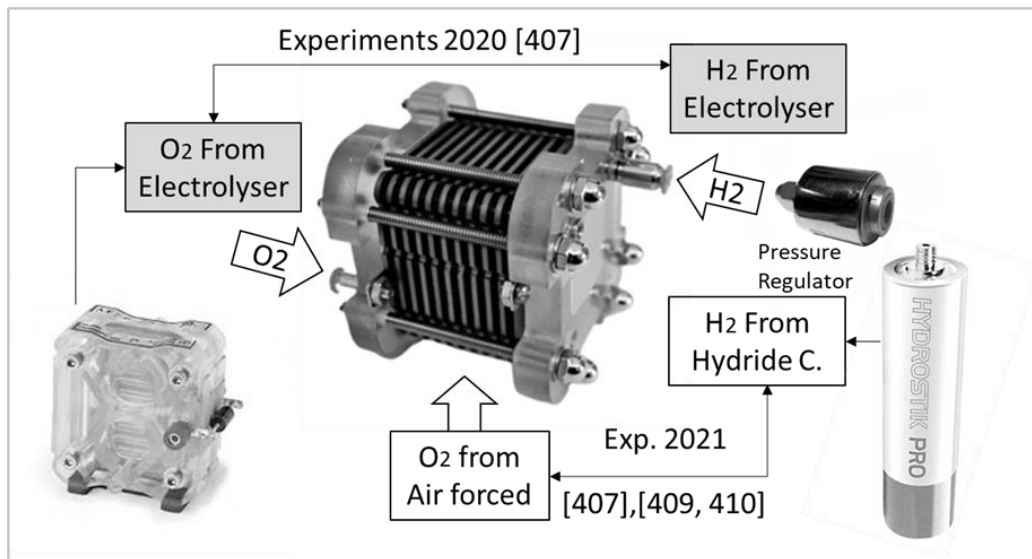


Fig. 6.4 Fuel cell, hydrogen, and oxygen supply in 2020 and 2021 tests [614]

Better oxygen (or air) flow significantly improves PEMFC power. Experiments demonstrated that the fuel cell equipped with IM-BP injection-molded polymer composite bipolar plates allowed charging a mobile phone battery up to 3.5 volts. The fuel cell assembly consisted of end plates made of milled PMMA, electrical contacts made of chrome-plated steel, PTFE gaskets, a GDL diffusion layer made of graphite cloth, MEA with DuPont Nafion 212 membrane covered with 0.4% Pt, and the CM-BP and IM-BP bipolar plates respectively. The fuel cell stack tests indicated a 355mW power (Table 6.3). A higher content of graphite added to the thermoplastic matrix positively influences the performance of the fuel cell, and similar results were found for both bipolar plates (CM-BP and IM-BP). However, they did not show the same electrical conductivity values.

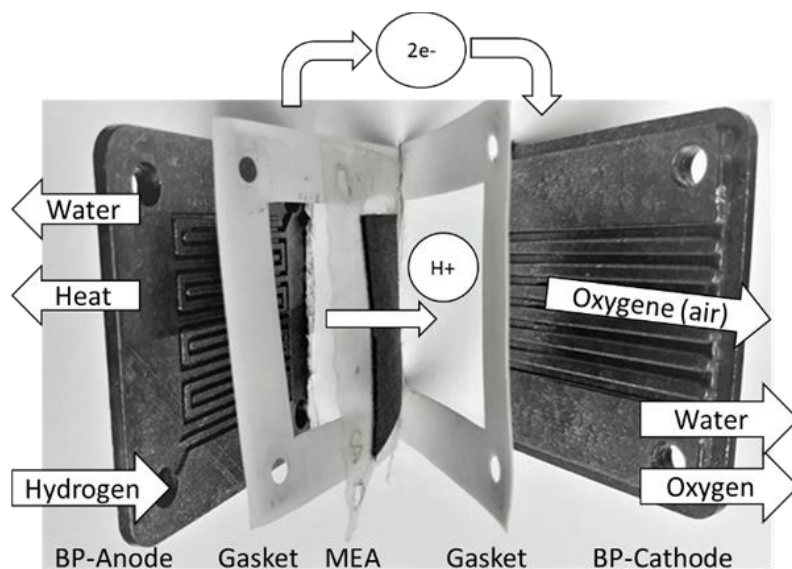


Fig. 6.6 shows the gas flow. The fuel cell contains BP-Anode, Gasket made of Teflon, MEA (Assembly - Polymeric Membrane – Electrode), Gasket, and BP-Cathode. In the fuel cell, oxygen from the air is reduced at the cathode and hydrogen at the anode. When passing through the membrane, the hydrogen molecules break down into protons and electrons due to the electrochemical reaction assisted by the catalysts.

Fig.6.6. PEMFC - converting chemical energy into electrical energy

In 2021, experiments with the 5cell PEMFC, H₂ supply AB₅ hydride (La_{10.5}Ce_{4.3}Pr_{0.5}Nd_{1.4}Ni_{60.0}Co_{1.27}Mn_{5.9}Al_{4.7}), O₂ from the air and help of a fan (Fig.6.4), equipped with the two types of bipolar plates demonstrated results close to the supplier's indicated ones (Fig. 6.8).

Table 6.3 Performance of the hydrogen fuel cell supplied by electrolysis [407]

<i>Fuel cell stack equipped with:</i>	<i>IM-BP</i>	<i>CM-BP</i>
Open circuit Voltage [V]	3.92	4.20
Operation Voltage [V]	3.45	3.44
Current [A]	0.100	0.089
Battery charged voltage /10 min. [V]	3.45	3.44
Power [W]	0.345	0.306
Hydrogen [MPa]	-	-
Electrical resistance [Ω]	1.5	1.5

Table 6.4 Fuel cell performance with hydrogen supplied from alloy cartridge AB_5

Model BP	Current [A]	Current density [mA/cm ²]	Voltage [V]	Power [W]	Debit Hydrogen cc/min
<i>CM-BP^a</i>	0.9	90	2.96	2.664	63
<i>IM-BP</i>	1.003	100	2.639	2.644	N/A

a. Data kindly provided by Dr. Matthew Mehmet Crawford, Fuel Cell Store, Texas, USA

Hydrogen loading was accomplished by electrolysis using a PEM device purchased from Horizon, Korea [614]. Hydrogen is a gas with high penetration and diffusion capacity through various metallic materials, and AB_5 alloy is specially designed to store hydrogen safely [615].

The fuel cell obtained a maximum power of 2664 mW at a current density of 100 mA/cm². The results were promising, as the supplier indicated for the cell equipped with CM-BP a power of 2664 mW at a current density of 90 mA/cm² and a hydrogen flow rate of 63 cc/min (see Table 6.4 and Fig. 6.8). Moreover, the results confirmed the importance of hydrogen. Although the conductivity evaluated with a simple device demonstrated superior conductivity for CM-BP (87S/cm) compared to the IM-BP one(41S/cm), the fuel cell performance was similar.

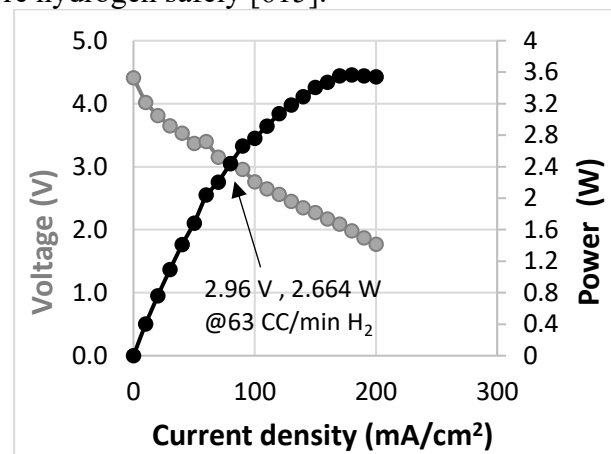


Fig. 6.8 The performance of the 5-cell fuel cell depending on the hydrogen supply (according to the supplier's data, Fuel Cell -note (a) Table 6.4)

6.5. 2020 MM+LBM Experiments, Results, and Discussion

The contact interface between bipolar plates and gas diffusion layers can influence voltage losses. The contact deformation resulting from the application of pressure between the polymer composite bipolar plates and the gas diffusion layer (made of graphite paper or graphite cloth) depends on the complex topography of the surfaces, the mechanical stresses at the interface being in the elastic or plastic range, in depending on the value of the tightening force of the assembly. The plastic deformation of the asperities with the highest height determines the contact area of two metal surfaces. We designed an experiment to test the complex sequential micro-milling - laser processing system MM+LBM for texturing the hydrogen discharge areas at two different cavity surface qualities. The mold made in aluminum 7075 was built with one cavity textured at a roughness Ra of 0.71 μ m and the second cavity Ra of 9.9 μ m.

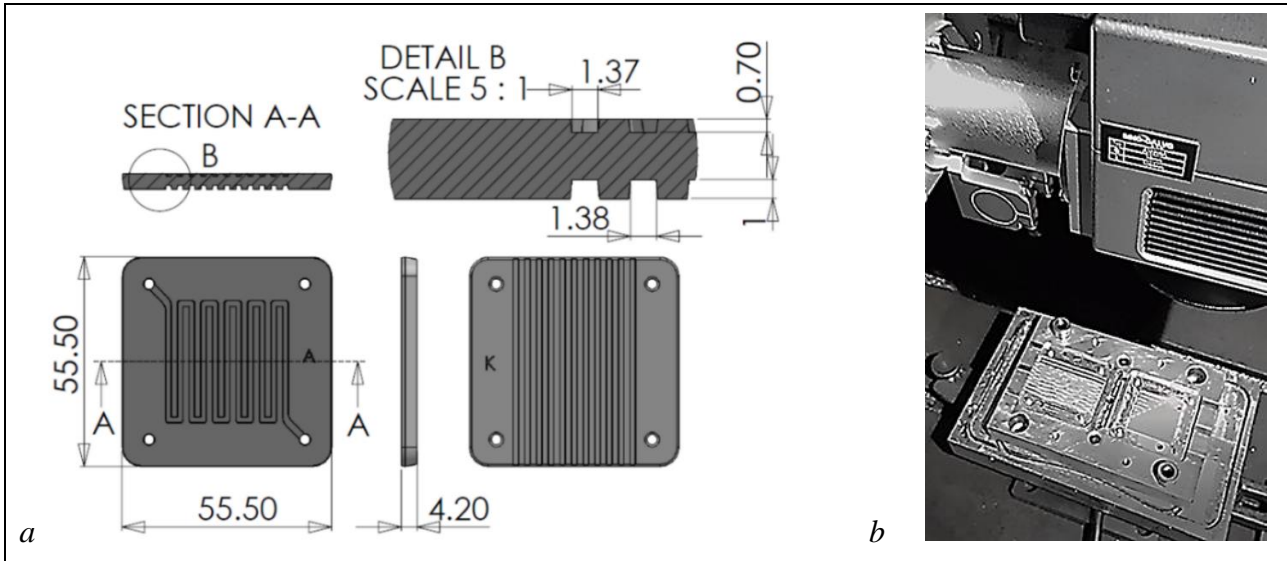


Fig. 6.9 a) 2020 Bipolar plate model – single gas circuit at the anode; b) The complex system used during laser processing [408]

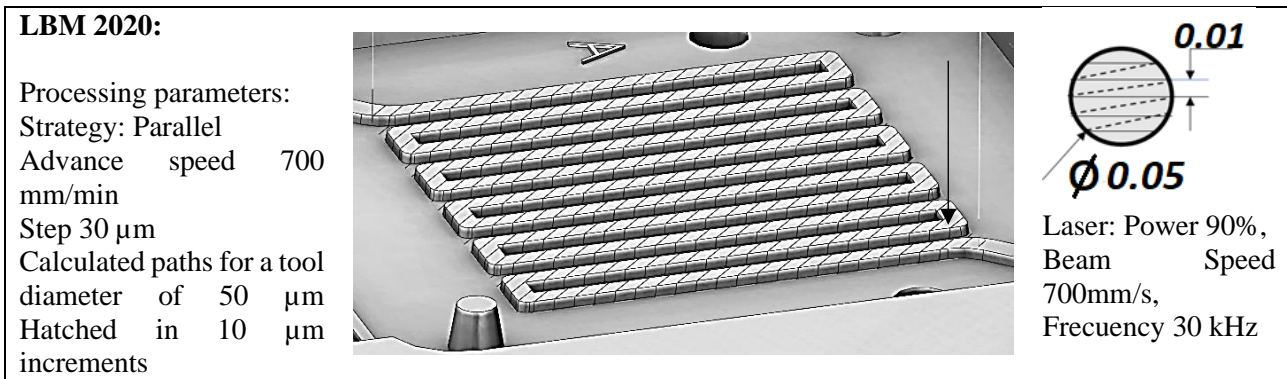


Fig. 6.10 LBM 2020 Experiment

6.5.1. The influence of surface roughness on electrical contact resistance

The contact BP roughness Ra 9.9µm - collector Ra 0.8 µm demonstrated an electrical resistance of about 50% of the contact BP Ra 0.71µm - collector 0.8 µm. It confirms the influence of roughness on the electrical contact resistance. The results presented in Fig. 6.13. demonstrated that the pressure applied to the surfaces influences the electrical contact resistance. (Fig. 6.14).

A combination of rougher surfaces with higher roughness helps reduce electrical resistance. The experiments carried out in the doctoral thesis observed the effects of plastic and elastic deformation of the surfaces in contact on the electrical resistance, which decreases by increasing the applied pressure. (Fig. 6.13)

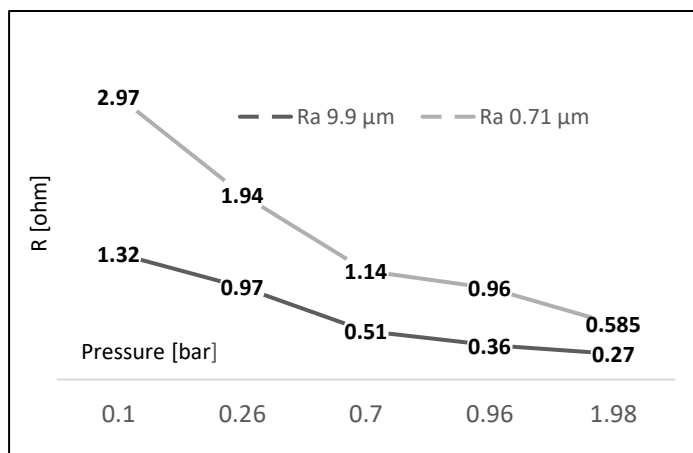


Fig. 6.13 Electrical resistance of contact CC-BP-CC on different pressure [408]

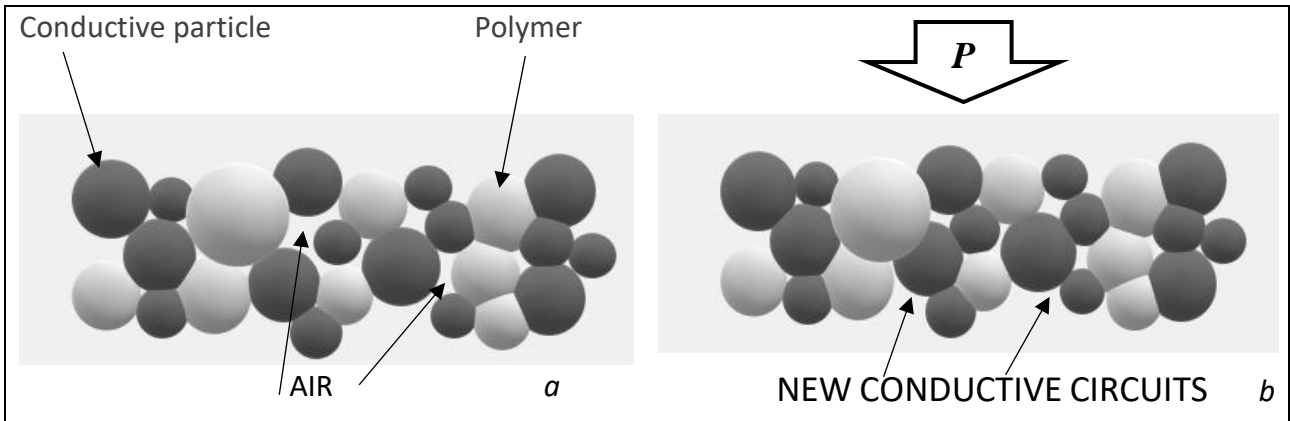


Fig. 6.14. The complex effect of pressure on electrical resistance

6.5.2 Study of the electrical resistance of a BP-GDL assembly

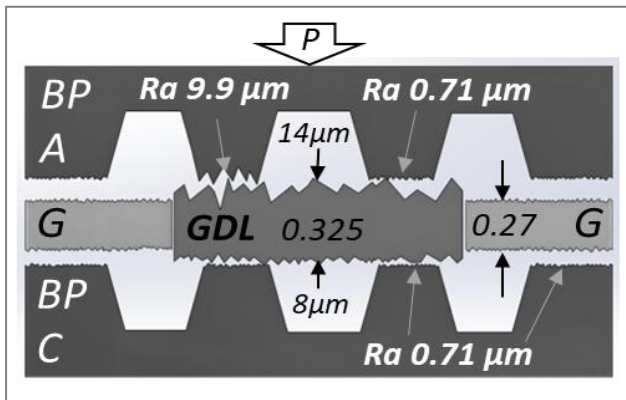


Fig. 6.15 Electrical resistance measurement method: BP-A, Bipolar Plate at the anode with Ra 9.9μm and Ra 0.71μm; GDL – gas diffusion layer; G, PTFE gasket; BP-C, BP at cathode Ra 0.71μm

We used a simple method to evaluate the contact resistance in the functional assembly CP-CC-BP-(GDL+G)-CC-CP (see Fig. 6.12. 6.15), including the gas diffusion layers and gaskets, at various loads. The assembly CP-CC-5x(BP-(GDL+G))-CC-CP were evaluated, too, at fastening screw tightening torques from 0.4 to 1 Nm. The novelty of the method, which we claim here, consists of the measurement of the electrical resistance with the simulation of a fuel cell assembly: bipolar plates, the GDL diffusion layer, and G gaskets, with the limitation of the compression range of the GDL. The gas diffusion layer has a thickness of 0.325 mm at a pressure of 0.0034 MPa and 0.28 mm at a pressure of 1 MPa.

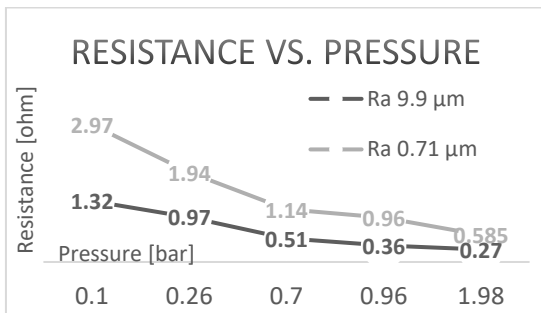


Fig. 6.16 Electrical resistance for one cell

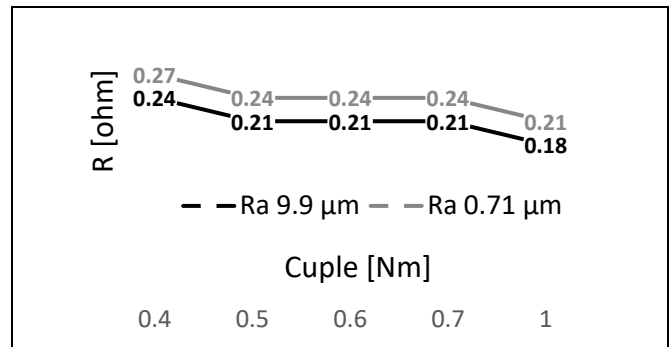


Fig. 6.17 Electrical resistance for one cell (measured in a set of 5 cells)

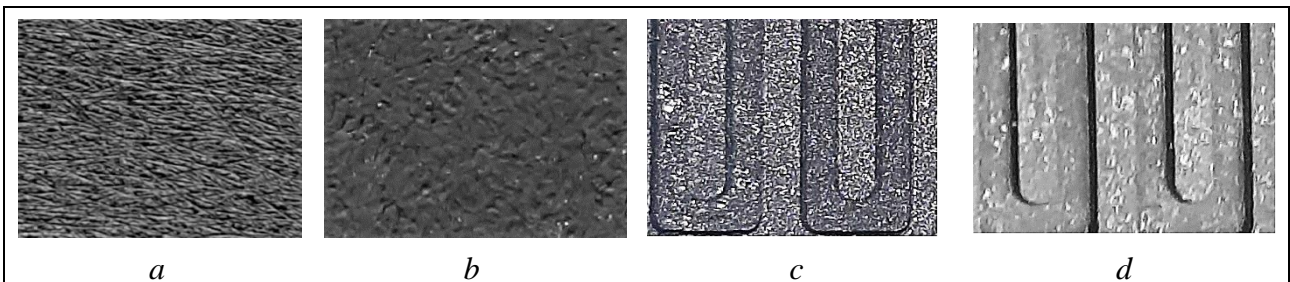


Fig. 6.18 Details of the surfaces a) GDL carbon fiber paper b) GDL- face covered with PTFE; BP at anode Ra 9.9μm d) BP at anode Ra 0.71μm

În Fig. 6.26 shows the diagram of microcontacts between the surfaces. The anisotropy of the roughness of the laser-finished surfaces (R_a 8.75 μm in one direction and 11.075 μm the perpendicular) and the surface roughness of the collector achieved by grinding (R_a 0.155 μm /0.21 μm) is noticeable. For the BP average R_a 9.9 μm combination, we can explain the electrical resistance decrease by increasing the real contact surface (Fig. 6.26).

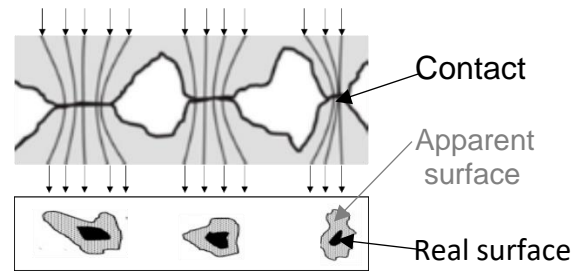


Fig. 6.26. The real microcontacts surfaces and the current flow.

6.5.3 Influence of the BP surface quality on the performance of the fuel cell stack

Experiments with the 5cell PEMFC, H_2 supply AB_5 hydride, O_2 from the air with the help of a fan, equipped with the two types of bipolar plates gas flow roughness, demonstrated better performance, a power of 2.7567 W for the IM-BP of R_a 9.9 μm versus 2.614 W for the IM-BP of R_a 0.71 μm . It confirms the results of the electrical contact measurements.

On the occasion of the expansion of the hydrogen supply resources, we tested the performance of the fuel cell assembled with bipolar plates having the roughness R_a on the anode surface of 9.9 μm and 0.71 μm , respectively. Tables 6.5 and 6. 6. Show the results of ten recordings at an interval of five seconds. The better efficiency obtained with IM-BP with surface R_a of 9.9 μm (2.7567 W) compared to IM-BP with R_a of 0.71 μm (2.639 W) can be explained by the lower electrical resistance (see Fig. 6.14) but also by the fact that the rough surface at R_a 9.9 μm in combination with the porous layer of the electrode (GDL covered with Teflon) contributes to the realization of additional hydrogen circuits and thus allows the gas discharge surface to be increased.

6.6. Conclusions regarding the complex laser processing system

The complex system milling – laser micromachining demonstrated good performance. Controlled with the *EZCAD2* application, the laser source through the 2D scanner and the f-theta lens scanned the pulsed beam as a circle of diameter 0.03 and hatched at a step of 0.02 mm with a speed of 800 mm/s. The laser beam replaces a physical tool working on G-code paths on the vertical machining center, with a feed speed of 800 mm/min, with a "parallel" strategy, step 0.03 mm (Experiment E1, see Fig. 6.2c). Depending on the process parameters, different surface qualities can be obtained. The new method using a LASER beam as a "tool" can be industrially implemented under reasonable conditions; the costs for a 20 Watt fiber laser for marking/engraving are currently around 4000 Euros (economic solutions). Moreover, we mention:

- Performing micro milling with a LASER beam as a "tool" represents a novelty in this field;
- The hydrogen fuel cell equipped with IM-BP manufactured with the new processing system can be used in portable, didactic applications;
- The performance of a fuel cell depends on the hydrogen supply, pressure, flow, sealing, the electrical conductance of the bipolar plates, and the quality of the MEA (polymeric membrane-electrode) assembly. During the tests, it was observed that a better flow of oxygen (or air) significantly improves the power provided by the fuel cells.
- Evaluation of electrical contact resistance of an assembly of BP with different roughness, GDL, and gaskets, to which a certain pressure is applied and restricted to the compressible domain of GDL, demonstrated lower electrical resistance for rough surface combination.

6.7. Laser processing system validation

The laser beam machining system as a "tool," developed by the author of this thesis, was tested and validated for processing in three dimensions and various materials. Fig. 6.27 and Fig.6.28 – a detail, show laser beam machining as a “tool” of a channel with a trapezoidal section, bases of 1 mm, respectively 0.8 mm, height 1 mm of an injection mold. It produces a box cover and lid for a methane gas safety sensor of about 10000 sets per year. The working parameters were established on the occasion of a previous experiment with processing the same channel in a flat steel plate: strategy in 2 ½ axes pocket laser “milling,” with a processing depth of 0.02 mm - and with a feed rate of 250 mm/min on paths generated for a tool with a diameter of 0.1 mm, in our case – the laser beam moving on a hatched circle with a pitch of 0.01 mm at a speed of 800 mm/s.



Fig. 6.27 Complex system – laser pocket milling steel DIN 1.2714

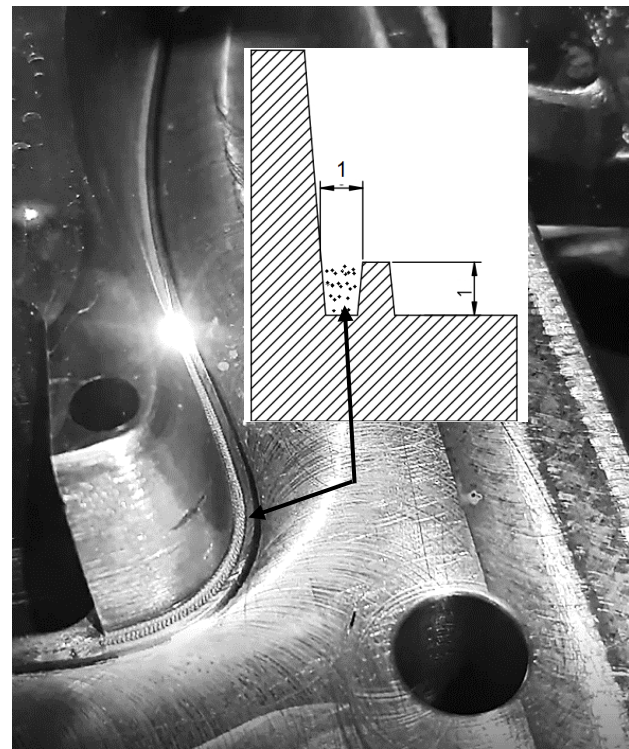


Fig. 6.28 Detail of laser micromachining 2 ½ „pocket” strategy

The system has demonstrated the possibilities of processing and implementation in industry. Traditionally, manufacturing a channel with this configuration required an insert solution, or electrical discharge machining, involving much labor. Laser processing spent 5 hours for "roughing" with 90% of the maximum power (20 W), pulse duration 120÷150 ns @30kHz with a maximum pulse energy of 0.67mJ at 30kHz and two hours finishing with a contouring strategy, and the laser beam at a power of 20% (from 20W). That demonstrated a strategy of a laser “cleaning” operation between the ablations at high power helps increase productivity. Improving the positioning of the reference of the laser beam to the workpiece is a challenge for future research activities.

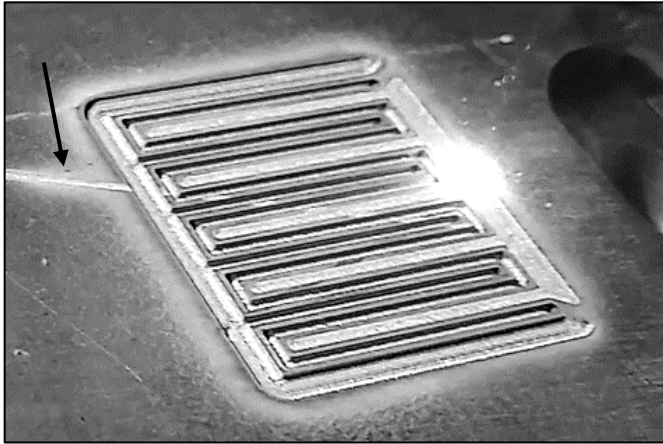


Fig. 6.29 Pocket laser milling

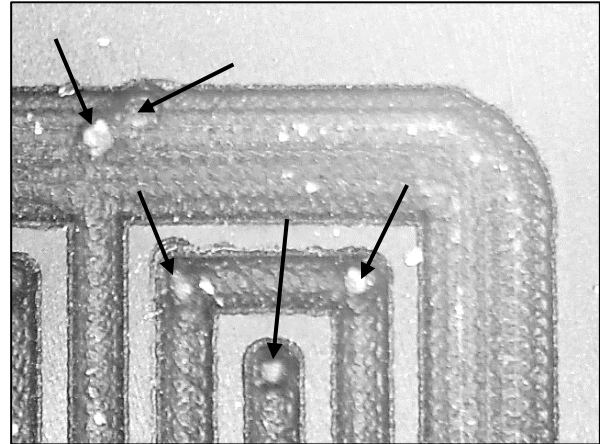


Fig. 6.30 Detail of tool engagement

Fig. 6.29 and the detail of Fig. 6.30 show the complex system processing of a microfluidic platform's channels. The channels have a section of 0.38 mm x 0.3 mm; the roughing pocket strategy generated tool withdrawal and engagement paths, respectively, indicated by arrows in Fig. 6.28, 6.29, additionally processed unnecessary areas. Thus, the correlation between laser beam generation and tool engagement displacement (similar to 3D printing, the beam must stop at G0 rapid traverses, retraction/engagement, and tool repositioning functions) is a direction for future research.

Fig. 6.31 shows a graphite electrode during laser processing with a "milling" strategy on vector paths projected on the surface ("*projection*"). Previously, the electrode was finished by CNC milling; paths were developed on a 3D CAD model.

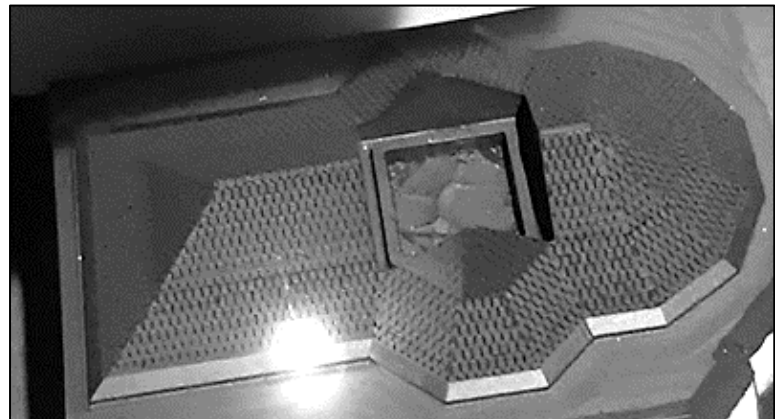
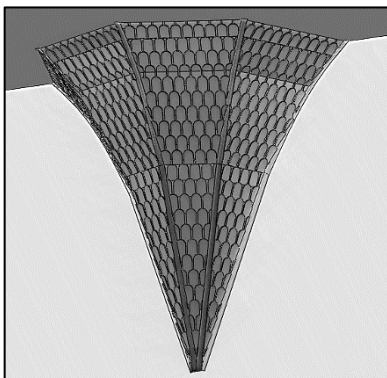
Fig. 6.31 Laser "*projection*" milling

Fig. 6.32 3D model section

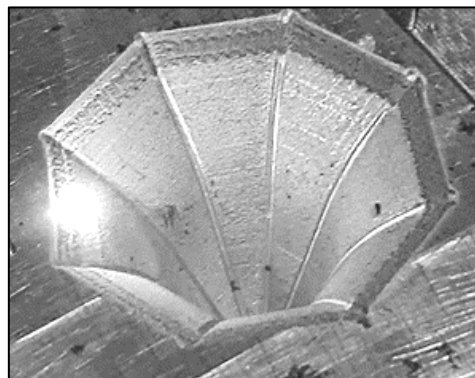


Fig. 6.33 Laser "milling" – contour strategy, Aluminium EN7075

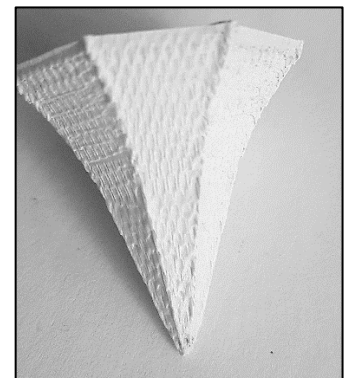


Fig. 6.34 Injection Molded Product

Fig. 6.33 shows the image of the cavity processing of an EN 7075 Aluminum alloy mold (Fig. 6.32 - a section through the 3D model), with the complex system with a laser processing strategy by contouring ("*contour*"). The perfect replication (Fig. 6.34) of the injection molded product into recycled and granulated PS demonstrated the system's good performance in an industrial application.

Chapter 7. Influence of process parameters on the electrical conductivity of injection molded polypropylene-graphite composite products

7.2 Materials, Equipment, and Methods

7.2.1 Materials

First, the bipolar plate was injection molded in a PP, Polypropylene grade J1100 from Rompetrol (MFR of 26,0- 30,0 g/10 min, 230°C, 2.16 kg/ISO 1133 B) for evaluation of the injection molding parameters: the temperature at injection unit nozzle, the temperature of the mold cavity, injection pressure and cavity pressure.



Fig. 7.1 The bipolar plates injection molded in PP87GR (model shown in Fig. 6.9a)

Then, we tested by injection molding polypropylene-graphite composite PP87GR with an 87wt% inorganic content, purchased from the Centre of Fuel Cell Technology ZBT GmbH Duisburg. The material is suitable for bipolar plates for low-temperature operated fuel cells (under 120 °C). Experiments used four sets of parameters on an L4 orthogonal array arrangement. The injection pressure was estimated with equation (7.3).

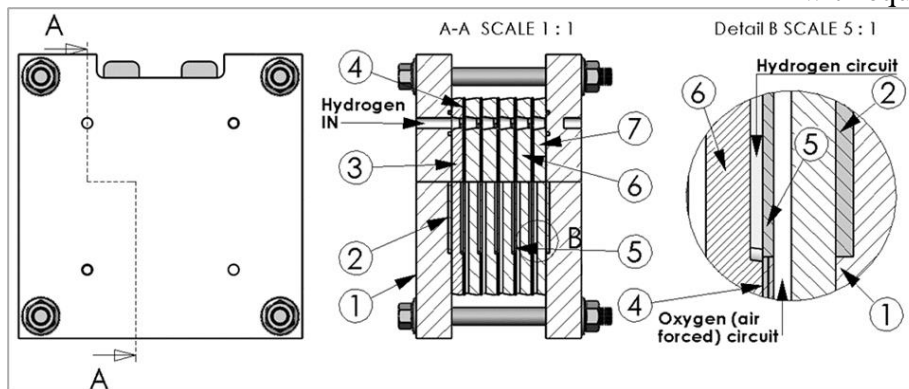


Fig. 7.2 PEM (Proton-Exchange Membrane) Fuel cell test assembly: 1) Endplate Anode side; 2) Copper Collector; 3) Anode Endplate; 4) Gasket; 5) Polymer Membrane Electrode Assembly; 6) Bipolar Plate; 7) Cathode Endplate

The measurement of the fuel cell efficiency equipped with the bipolar plates of the four experiments directly indicates the influence of the injection molding parameters. Four bipolar plates of each experiment were assembled in a hydrogen-air (forced) fuel cell stack, as shown in Fig. 7.5. The fuel cell stack was tested at room temperature, and hydrogen was supplied from an AB₅ hydride cartridge at 0.3 bar.

7.2.4 Estimate the Injection Pressure Method

There is a correlation between injection pressure and composite viscosity; based on the equation of Dobrescu et al. (7.1), a formula was adapted with the introduction of a correction factor given by the influence of processing temperatures (7.3):

$$p_{hk} = p_{hp}(1 + ac^b/d^f) \quad (7.3)$$

where: p_{hk} is the hydraulic injection pressure of the composite, p_{hp} the matrix polymer's hydraulic injection pressure, $a = 0.297$ and $b = 1.3$, are experimentally evaluated by Dobrescu et al. [709], $f = 2.5$, coefficient experimentally evaluated by considering the influence of the combined temperatures of the melt at the nozzle and mold temperature, d , calculated with equation (7.4):

$$d = (T_{Nozzle\ k} + T_{Cav\ k}) / (T_{Nozzle\ p} + T_{Cav\ p}) \quad (7.4)$$

where: $T_{Nozzle\ k}$ is the (nozzle set) temperature of the composite, $T_{Nozzle\ p}$ is the (nozzle set) temperature of the polymer, $T_{Cav\ k}$ is the mold cavity temperature for the composite, and $T_{Cav\ p}$ is the mold cavity temperature for the polymer, as recommended by suppliers.

Table 7.3. Procedure for choosing the levels of the factor's temperature and pressure.

Factor	Composite Supplier Recommendation	Observation
Set Temperature at Nozzle (T_{Nozzle})	$T_{Nozzle} = 300 \div 360^\circ\text{C}$ Average $T_N = 330^\circ\text{C}$	For polypropylene, the AVERAGE Barrel's Nozzle Temperature for PP is about 220°C ;
Mold Cavity Temperature (T_{Cav})	$T_{Cav} = 70 \div 80^\circ\text{C}$ AVERAGE $T_C = 75^\circ\text{C}$	For polypropylene, the AVERAGE Mold Temperature is about 30°C ;
Injection Pressure (p_{hk}) [bar]	High pressure. It was chosen, $p_{hk} \pm 15\text{ bar}$, 100 and 130 bar	Applying formula (8.7) $p_{hk} = p_{hp} \left(1 + \frac{ac^b}{df}\right)$ For values of $a = 0.0295$ and $b = 1.3$ [710], $d = (330 + 75) / (220 + 30)$, $f = 2.5$, $p_{hp} = 30$ bar results $p_{hk} = 115$ bar.

7.5 Results and discussions

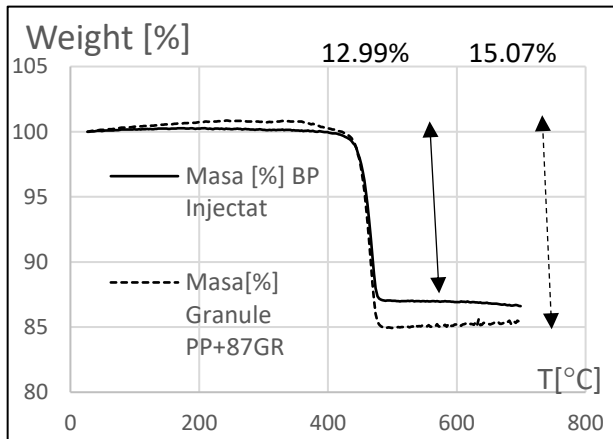


Fig. 7.10 TGA analysis on a ten °C / minute profile

No polymer is infinitely stable at processing temperatures, so property change and degradation can be accurately estimated [714]. Thermogravimetric analysis (TGA) of the PP87GR composite presented in Fig. 7.10 was performed on a NETZSCH TG 209F1 Libra® instrument [423] at the Advanced Polymer Materials Group, Politehnica University of Bucharest. TGA analyses were performed on samples of the PP87GR composite taken from injection-molded BP and granules and indicated a high rate of degradation of the PP87GR composite above 430°C .

Table 7.10. Taguchi analyses on SN Ratio for *Larger-The-Better*, Conductance ($G = I/R$)

Factors →		Temperatures [°C]				p_h Pressure [Bar]		tH Holding Time [s]	
Levels		Level 1		Level 2		Level 1	Level 2	Level 1	Level 2
Experiment	S/N -ec.(7.10)	320	70	340	80	100	130	4	8
I	8.293	8.293				8.293		8.293	
II	10.022	10.022				10.022		10.022	
III	12.369	12.369				12.369		12.369	
IV	13.294	13.294				13.294		13.294	
$S/N_{level\ 1} + S/N_{level\ 2}$		18.315		25.663		20.662		21.587	
$(S/N_{level\ 1} + S/N_{level\ 2})/2$		9.1575		12.831		10.331		11.195	
Factor influence		3.674				1.327		0.402	
Rank		1				2		3	

Our experiments observed that the temperature favors the contact between the conductive graphite particles embedded in the polymer matrix, thus creating several conductive circuits that improve the electrical conductance. As shown in Table 7.15, Fig. 7.14, and Fig. 7.15, energy efficiency measurements confirm the influence of injection unit (material-level) and mold temperatures on the bipolar plate and fuel cell performance.

Table 7.15 The power efficiency of the fuel cell with each of the four experiments bipolar plates.

Exp.	Composite	Pressures [bar]			Temperatures [°C]		Power [W]	Efficiency
		p_c^*	p_h^*	p^{***}	T_{Cav}	T_{Nozzle}		
I	PP87GR	99	100	807	70	320	2.235	100%
II	PP87GR	189	130	1050	70	320	2.69	115%
III	PP87GR	188	100	807	80	340	2.86	122%
IV	PP87GR	300	130	1050	80	340	3.14	134%

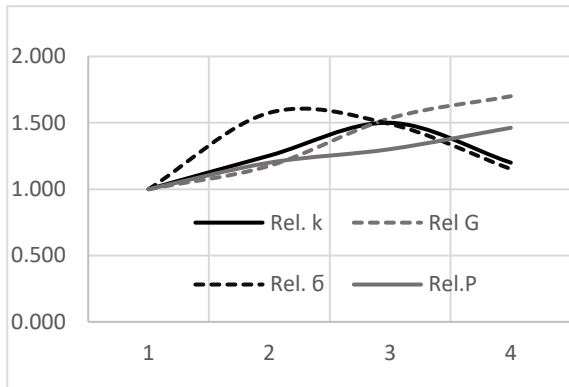


Fig. 7.14 Relative k , G , σ , P

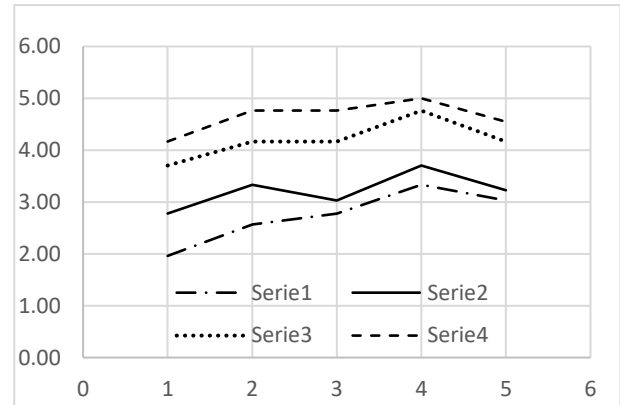


Fig. 7.15 BP Thickness

7.6 Conclusions regarding the influence of process parameters on the electrical conductivity of injection molded products

Taguchi and ANOVA analyses on an L4 orthogonal array demonstrated a dominant influence of injection pressure on BP mass and thickness and the critical contribution of process temperatures on electrical conductance. The thermogravimetric analysis confirmed the inorganic content and degradation temperatures.

- Better packing allows for reducing the interstices between conductive particles and thus creating additional conduction networks;
- Higher cavity pressure on the conductive particles can create better electrical contact through the molten polypropylene layer;
- The properties of the constituent materials are not automatically and guaranteed transfer to the resulting composite material and the product manufactured with it;
- We opted for estimating the injection pressure using a thermodynamically adapted Dobrescu formula. The pressure measured in the cavity confirmed the new methodology, which can be applied successfully and with minimal costs.
- For the estimation of electrical conductivity, an approach based on the principles of phase balance could contribute to obtaining good results.

Chapter 8. Thermodynamic evaluation of polymer-carbon hybrid composites conductivity

This chapter analyzes the influence of injection molding parameters and inorganic content on electrical conductivity in a thermodynamic approach. The work describes the development of low-cost conductive polymer composites for injection molding bipolar plates (IM-BP). Black masterbatch granules (polyethylene-carbon black) were mixed with expanded graphite (EG). (Table 8.3)

Table 8.3 Composite recipes, volume concentrations recalculated on samples

Composite	LDPE wt[%]	LDPE Vol[%]	CB wt [%]	CB vol[%]	EG wt[%]	EG vol[%]
C1	51.00	68.82	49.00	31.18	-	
C2	43.15	62.33	41.45	28.25	15.4	9.42
C3	38.10	57.70	36.60	26.10	25.30	16.20
C4	30.60	53.60	29.40	24.30	40.00	22.10

The bipolar plate has the role of electrical transport within the fuel cell assembly; therefore, we have chosen the model of Bueche, which considers the network chains are parallel conductors through the polymer [148]. We explored the correlation between process parameters and electrical conductivity, estimating the effect of thermodynamic state transformations on the fraction of volume of particles participating in the chains of the conductive network. In this experiment, expanded graphite was added to a conductive composite (a low-density polyethylene matrix + carbon black), the Bueche model (chapter 1 and equations 8.8a,b,c) being completed with a correction factor which takes into account the volume fraction of the particles participating to the networks ω_g , respectively correlated with the temperatures of the process, in reasonable agreement with the behavior observed in the experiments carried out in this study. Therefore, we propose the following variant of the Bueche equation with a modified fraction ω_{gf} :

$$\rho/\rho_m = 1/[1 - V_p + V_p \omega_{gf}(\rho_m/\rho_p)] \quad (8.9)$$

$$\omega_{gf} = \omega_g \cdot f \quad (8.10)$$

Taguchi analysis (according to chapter 7, Table 7.10) found out for injection molding the PP87GR composite, the contribution of temperatures is 68%, injection pressure 25%, and holding time 7%. As a result, one can consider a correction factor f , estimated with the relation:

$$f = 1 + 0.68 \cdot \frac{TMci+TCci}{TMm+TCm} + 0.25 \cdot \frac{Pck}{Pcm} + 0.07 \cdot \frac{tHci}{tHcm} \quad (8.11)$$

Equation 8.9, rewritten to calculate electrical resistance:

$$R/R_m = 1/[1 - V_p + V_p \omega_{gf}(R_m/R_p)] \quad (8.12)$$

8.3 Results and discussions

Bipolar plates were injection molded in the conductive composite four recipes, recording the cavity pressure, mold, and material temperatures. Results observed that the manufacturing method significantly influences the combination and transfer of constituent material properties to the final product. Conductive particles added to a matrix that has a certain intrinsic conductivity contribute to networks by combining with some of the particles isolated from the base matrix and under the influence of process parameters (Fig. 8.7). Thermodynamic approach of the influence of process parameters on product properties can explain the phenomena.

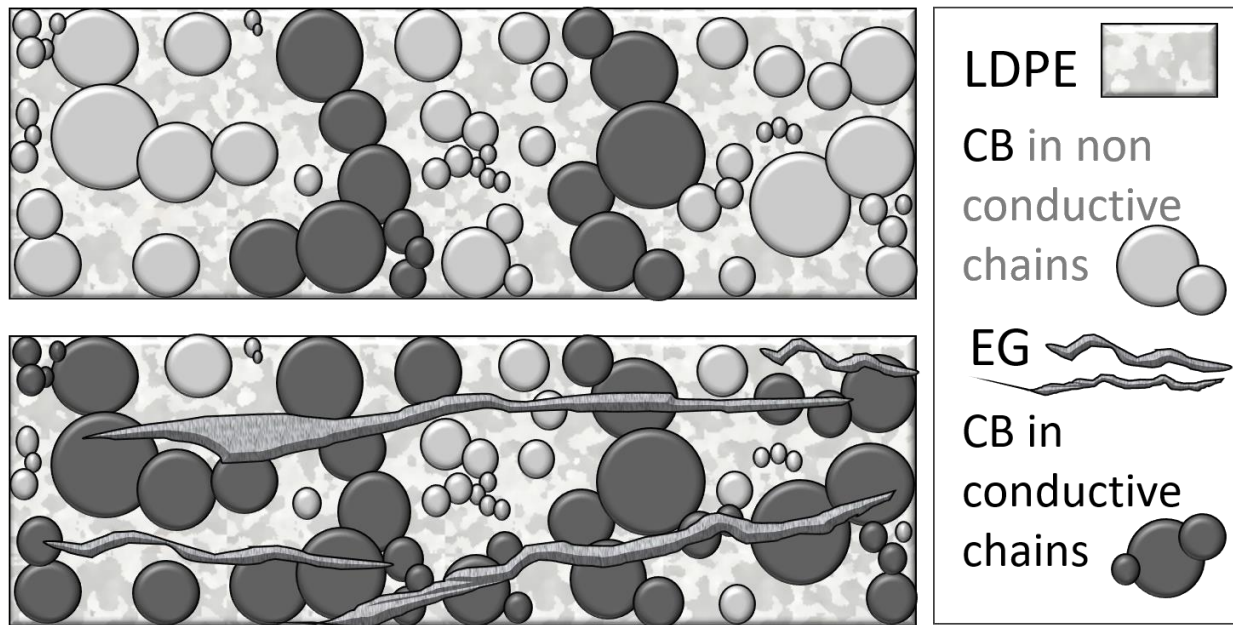


Fig. 8.7 Formation of new conducting networks with the participation of CB isolated particles.

The situation differs, however, in the case of applying pressure to the composite assembly subjected to the electrical resistance test. This explanation is based on a possible mechanism for creating new conductive networks because the thermoplastic matrix is compressible. Due to the additional forces applied, different distributions of mechanical stresses at the level of the constituent particles of the composite introduce localized compaction effects. The process temperatures, cavity pressure, and holding time evaluated the value of the coefficient f . Process temperatures significantly influence the pressure and, implicitly, the compaction of the powders in the polymer matrix, contributing to the increase of the electrical conductivity, in good agreement with the observations that confirmed the reduction of the resistivity of the powders with the application of mechanical pressure. For $\omega=0.64$ and $R09C1=1.494 \Omega$ resulted lower electrical resistances $R_{EGC3}=0.0869 \Omega$ și $R_{EGC4}=0.0889 \Omega$ (Fig. 8.8. și 8.9).

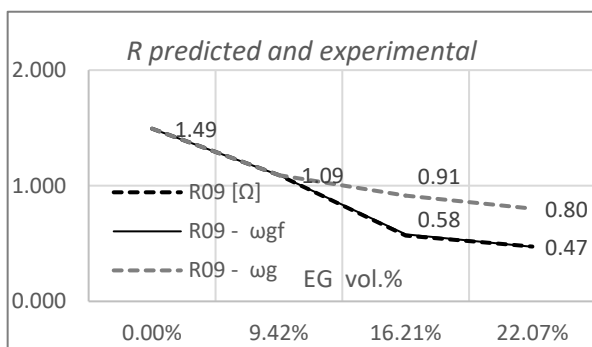


Fig. 8.8 Electrical Resistance (--- experimental --- predicted).



Fig. 8.10 Injection Molded Bipolar Plates, sample nr. 27 cathodes, nr. 26 anodes (C3 recipe)

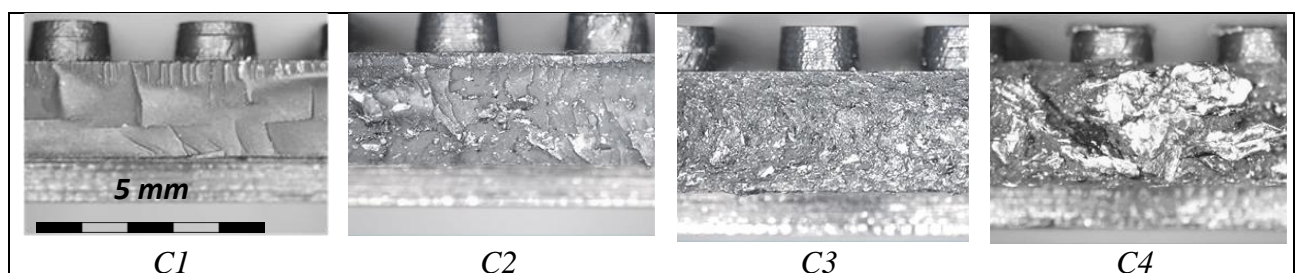


Fig. 8.13 Images of injection gate fracture - IMBP recipes C1, C2, C3 și C4.

The fuel cell equipped with the C4 composite injection molded BP demonstrated the best performance, comparable to that of the PP87GR recipe (Ch.6, Ch.7.). The efficiency of the PEMFC equipped with BP-C4 compared to that of BP-C1, indicates an essential contribution of expanded graphite to the reduction of ohmic losses. The fuel cell's power behavior is similar to the conductance BP (*I/R09*) and the thermal conductivity factor (Fig. 8.14). The electrical resistivity of the CB resulted in $\rho_{CB}=0.324 \Omega\text{cm}$ for $\rho_{CI}=2.08 \Omega\text{cm}$.

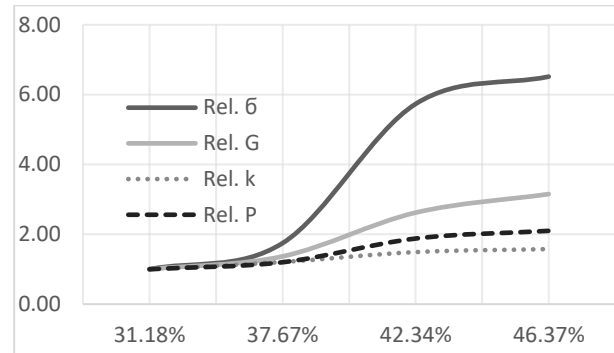


Fig. 8.14 Relative conductivity, conductance, and power for the four experimental polymer composite recipes.

8.4. Economic highlights

A PEMFC delivering a current density of 1 A/cm^2 and a voltage per cell of 0.65 V can be built with 20 bipolar plates with a gas discharge area of 50 cm^2 and a total surface of 100 cm^2 . At a minimum thickness of 3 mm and a density of 1.5 g/cm^3 (for example, the composite PP87GR, Chapter 7, and [409]), we obtain a total mass of $100 \cdot 0.3 \cdot 1.5 \cdot 20 = 600 \text{ g}$. At a thickness of 2 mm (difficult to injection mold it), 0.4 kg could be achieved. Injection molding at a 25 Euro/hour rate at a total cycle of 20 seconds could produce 180 bipolar plates per hour. The mold with one cavity could cost 5000 euros. The amortization rate of 100.000 BPs counts to one Euro per 1 kW . For 1 kW , 20 BPs manufacturing costs could achieve 2.77 Euro . One kW BPs in PP87GR, production costs are $10+1+2.77=13.77 \text{ Euro}$; One kW BPs in LDPE-CB-EG, production costs are $1+1+2.77=4.77 \text{ Euro}$. Thus, this evaluation proposes promising LDPE-CB-EG and PP-CB-EG composites and economical solutions to be further explored. Table 8.12 presents the prices used in our cost estimation.

Table 8.12 Materials costs, EX Works[822]

Pos.	Matrix	Composite	Filler	Price Euro/kg	Ref.
1	PP			2	
2	LDPE			2	
3			CB SFR	1.5	
4			EG	1.5	
5			GR	1.5	
6			MWCNT 20-30 nm >95%	95	[831]
7			GRAPHENE	32000	[831]
8	LDPE	LDPE-CB	(50%CB)	3.5	
9	PP	PP- CB	(40%CB)	3.5	
10	PP	PP87GR	(82%GR+5%CB)	25	

8.5. Conclusions regarding the thermodynamic analysis of the conductivity of polyethylene-carbon black-expanded graphite hybrid composites

- The polyethylene-carbon black-graphite composites demonstrated good electrical conductivity; Therefore, bipolar plates for fuel cells can be manufactured by injection molding common composite materials at much more advantageous prices than recipes using CNTs and graphene;
- When new fractions of conducting particles are added to a polymeric conductive matrix, the volume fraction contributing to the network can be corrected with a factor that considers the thermodynamics of the method (pressure, temperature, specific volume).

Chapter 9. Conclusions and contributions

The main objective consisted of *advanced technologies for texturing the mold cavity surfaces and their replication in the injection molding of thermoplastic composites, with an application in the energy field – bipolar plates for hydrogen fuel cells*. This Ph.D. thesis presents the results, author contributions, and conclusions on the advanced technologies for mold surface texturing, including additive processes and the injection molded products replication (Chapter 5); the development of a complex system for laser machining and the evaluation of the influence of surface texture on the physical properties (Chapter 6); optimization of process parameters and their influence on the properties of the product tested in the functional assembly (Chapter 7); thermodynamic correlations of process parameters and electrical conductivity (Chapter 8).

The specific objectives were:

Experimental study of micro-milling, photochemical machining PCM, laser beam machining LBM, electrical discharge EDM, additive manufacturing AM (BJT class ISO 52900);

Conclusions:

- **Laser micromachining** has become a standard technology. Laser texturing injection mold cavity surfaces is an accessible, economical method that offers new possibilities for product design and fabrication; research is directed to ultrashort (pico and femtosecond) pulse ablation. The nanosecond pulse laser ablation is a reliable alternative for specific applications.
- **Photochemical machining** is suitable for fabricating precision details but with limited depth and is still a successful method for mold texturing;
- **Electrical discharge machining EDM** is a standard method in the mold and die-making industry for surface finishing. The cavity surface EDM finish can be described by the designer and manufactured following VDI 3400;
- conventional and high-speed **milling** offers high surface finishing and good productivity;
- **Additive manufacturing methods** are becoming popular in prototyping and fabrication at reasonable costs of mold components.
- Laser and photochemical texturing patterns are usually image-type files (e.g., *JPEG, BMP*) and vector (e.g., *PDF, SVG, AI, DXF*). The machining paths for milling the cavities and EDM electrodes are calculated on the surfaces of 3D CAD models; “*image-to-surface*” algorithms help to transfer the natural object’s structure to the mold cavity; AM technologies use CAD files (e.g., *STL, OBJ*).

Contributions:

- The technologies were validated and demonstrated the domain of industrial integration: *LBM texturing* of an injection mold cavity with a pattern developed from an *image-type (JPEG)* file; *LBM engraving* (on the *image-type* pattern), *LBM drilling* and *LBM micro-milling* on a *vector-type* pattern of a thermoforming mold cavity;
- The author developed an algorithm combining the *image-to-plane surface* G-Code files to obtain the paths for machining a complex 3D surface. [407]

Development of a sequential system for complex processing by micro-milling and laser texturing;

Conclusions:

- The laser beam through the 2D scanner and the *f-theta* lens scans a hatched circle, describing a micro-tool moving on the CNC paths controlled by the vertical machining center. Depending on the process parameters, different surface qualities can be obtained.

Contributions:

- The new method developed by the author using the laser beam to replace a physical tool in CNC machining can be industrially implemented under reasonable conditions. The complex

system has been validated by short pulse laser processing different materials (steel, graphite, aluminum) with pocket, contour, or parallel machining strategies. (see 6.7)

Correlations between the process parameters and the quality of the laser-textured surfaces;

- Frequency, scanning speed, power, and hatch step influence the most laser textured surface.
- The replication rate of the corresponding injection molded product surface depends on the topography detail, process parameters, and shrinkage significantly influence.
- The nanosecond pulse laser demonstrated a reasonable ablation rate and was economical.

Effects of surface quality and process parameters on physical product properties;

Conclusions:

- A rough surface combination demonstrates a lower electrical contact resistance.
- The injection molding parameters influence the electrical conductivity of a polymeric conductive composite product; A thermodynamic approach can explain the phenomena.

Contributions:

- The new method to evaluate the electrical resistance in the entire functional assembly observed a better PEMFC performance when equipped with BP of the rough surfaces. It contributes to the design of the gas discharge areal topography for efficiency.
- The author proposes an adapted Dobrescu viscosity formula to predict the injection pressure needed for a highly filled polymeric composite. The method helps industrial engineers evaluate the process parameters when rheological data are unavailable.

Development of new economic thermoplastic conductive composites based on standard materials; Development of the injection molding technology of PEMFC bipolar plates.

Conclusions:

- Experiments with the injection molded BP in low-density polyethylene and polypropylene filled with carbon black and expanded graphite demonstrated promising results, good electrical conductivity, and an economical fabrication method to be industrially implemented.
- The volume fraction contributing to the network can be corrected with a factor that considers the thermodynamics of the method (pressure, temperature, specific volume).
- The physical properties of constituents are not guaranteed transfer to the resulting composite.

Contributions:

- Experiments with the injection-molded BP in the LDPE and PP author-developed recipes demonstrated a PEMFC efficiency comparable with the compression-molded conductive thermoset composite. It helps future investigations for better performance.
- Experiments with a fuel cell stack equipped with BP injection molded in a polypropylene-graphite composite observed the influence of the surface gas discharge and hydrogen and oxygen supply on the performance. With a ten square centimeter area and five cells, hydrogen (30 ml/min), and oxygen (15 ml/min) generated by electrolyzing, a PEMFC charged a mobile telephone battery up to 3.5V. It is a base for future explorations of fuel cell applications.
- The author suggests a thermodynamic approach to Bueche's electrical resistivity prediction model. The method helps industrial engineers optimize the process parameters for better electrical conductivity.

Further work

The author will continue researching the complex laser beam processing system to improve the correlation of the displacement on the CNC paths and laser beam generation. Also, to optimize the recipes of LDPE-CB-EG and PP-CB-EG composites by analyzing the effect of different types of carbon black and additives to obtain higher electrical conductivity and to develop new models of bipolar plates for better energy efficiency. The author will collaborate with the academic environment and will continue publishing.

Bibliography (extras)

- [101] Brydson JA. *Handbook for plastics processors*. ISBN 0 434 90200 4, Butterworth-Heinemann; **1990**.
- [102] *** https://www.bpf.co.uk/plastipedia/plastics_history/Default.aspx accessed **20220213**
- [103] *** <https://www.corvsport.com/the-c1-corvette-buyers-guide/> accessed **20220922**
- [104] *** https://ro.wikipedia.org/wiki/Dacia_500_Lăstun accessed **20220922**
- [105] ISO – the International Organization for Standardization, SR EN ISO 472-**2013** Materiale Plactice. Vocabular; SR EN ISO 472/A1(**2019**) Materiale Plactice. Vocabular. Amendament 1:Elemente suplimentare
- [106] Groover MP. *Modern manufacturing materials, processes, and systems*. Pennsylvania. **2010**.
- [148] Bueche F, J. Appl. Phys. **43**(11), **1972**, pp. 4837-4838
- [160] ISO – the International Organization for Standardization, SR EN ISO/ASTM 52900-**2022** Fabricație aditivă. Principii generale. Noțiuni de baza și terminologie
- [161] Schiller GF. *A practical approach to scientific molding*. Carl Hanser Verlag GmbH Co KG; **2018**.
- [186] DEX '16 Dicționarul explicativ al limbii române, ediția a III-a revăzută și adăugită, Academia Română, Institutul de Lingvistică „Iorgu Iordan”, Editura Univers Enciclopedic Gold, **2016**
- [187] Morgan T. The hydrogen economy: A non-technical review. (**2006**). United Nations Environment Program E.
- [188] *** Hydrogen and fuels cells for transport | Mobility and
https://ec.europa.eu/transport/themes/urban/vehicles/road/hydrogen_en (accessed **20210824**)
- [189] Spiegel, C. *Designing and building fuel cells*. Vol. 87. New York: McGraw-Hill, **2007**.
- [190] Chen Y, Eneanu L, Montalvão D, Sutharssan T. A Review of Computational Fluid Dynamics Simulations on PEFC Performance. Journal of Applied Mechanical Engineering. **2016** Dec 10
- [191] Larminie J, Dicks A, McDonald MS. *Fuel cell systems explained*. Chichester, UK: J. Wiley; **2003** Apr.
- [192] Ruge M, Büchi FN. Bipolar elements for PE fuel cell stacks based on the mold to size process of carbon/polymer mixtures. In Proceedings of the first European PEFC Forum (EPCF) **2001** (pp. 299-308).
- [194] Carcadea E, Ismail MS, Ingham DB, Patularu L, Schitea D, Marinoiu A, Ion-Ebrasu D, Mocanu D, Varlam M. Effects of geometrical dimensions of flow channels of a large-active-area PEM fuel cell: A CFD study. International Journal of Hydrogen Energy. **2021** Apr 9;46(25):13572-82.
- [195] Wilberforce T, El-Hassan Z, Khatib FN, Al Makky A, Mooney J, Barouaji A, Carton JG, Olabi AG. Development of Bi-polar plate design of PEM fuel cell using CFD techniques. International journal of hydrogen energy. **2017** Oct 5;42(40):25663-85.
- [197] Kopasz JP, Benjamin TG, Schenck D. 2017 bipolar plate workshop summary report. Argonne National Lab.(ANL), Argonne, IL (United States); **2017** Aug 17
- [198] *** , Flow field design, <https://www.fuelcellstore.com/blog-section/fuel-cell-materials-blog-articles/flow-field-design> (accessed **20210830**)
- [201] Brinksmeier E, Preuss W, Micromachining, Phil. Trans. R. Soc. A **370**, 3973–3992 doi:10.1098/(**2012**)
- [202] Groover MP. *Fundamentals of modern manufacturing: materials, processes and systems*, Forth Edition, USA: Jhon Wiley & Sons, **2010**.
- [203] Piljek P, Keran Z, Math M. Micromachining–review of literature from 1980 to 2010. Interdisciplinary Description of Complex Systems: INDECS. **2014** Jan 31;12(1):1-27
- [204] Jain VK, Patel DS, Ramkumar J, et al. Micro-machining: An overview (Part II). Journal of Micromanufacturing. October **2021**. doi:10.1177/25165984211045244
- [205] *** <http://www.artn.ro/> accessed **20211123**
- [206] ISO – the International Organization for Standardization, ISO 23020:**2021**(en) Space systems — Determination of test methods to characterize material or component properties required for break-up models used for Earth re-entry
- [209] ***[www.gfms.com/us/ Laser machining/GF Machining Solution](http://www.gfms.com/us/Laser_machining/GF_Machining_Solution), accessed **20220110**
- [210] *** <https://en.dmgmori.com/products/machines/lasertec/lasertec-shape/lasertec-75-shape> accessed **20220331**
- [211] *** <https://www.sciencedirect-com.am.e>
information.ro/search?q=microstructured%20surface accessed **20210820**
- [212] ISO – the International Organization for Standardization, EN ISO-4287:**1997** [201] Geometrical Product Specifications (GPS) – Surface texture: Profile method – terms, definitions and surface texture parameters
- [213] ISO – the International Organization for Standardization, SR EN ISO 21920-2:**2021** *Specificații geometrice pentru produse (GPS). Starea suprafeței: Profil. Partea 2: Termeni, definiții și parametri pentru starea suprafeței*
- [214] ISO – the International Organization for Standardization, EN ISO 25178-2:**2021**, Geometrical product specifications (GPS) – Surface texture: Areal – Part 2: Terms, definitions and surfaces parameters
- [215] VDI 3400 – **75** Electrical Discharge Machining (EDM), Definitions, Production, Application
- [216] Berglund J, Söderberg R, Wärmefjord K, Leach R, Morse E. Functional tolerancing of surface texture—a review of existing methods. Procedia CIRP. **2020** Jan 1;92:230-5.
- [224] *** <https://www.moldmakingtechnology.com/articles/surface-finish-understanding-mold-surface-lingo> accessed **20221229**

- [255] Piccolo L, Puleo K, Sorgato M, Lucchetta G, Masato D. Modeling the replication of submicron-structured surfaces by micro injection molding. *Materials & Design*. **2021** Jan 15;198:109272
- [281] Wan-Sik Woo, Choon-Man Lee, A study of the machining characteristics of AISI 1045 steel and Inconel, 718 with a cylindrical shape in laser-assisted milling, *Applied Thermal Engineering* 91 (2015) 33-42 (**2015**)
- [282] Z.Z. Dhokia, V.G. Nassehi, A review of hybrid manufacturing processes - state of the art and future perspectives, *International Journal of Computer Integrated Manufacturing*, vol. 26, no. 7, pp. 596615. <https://doi.org/10.1080/0951192X.2012.749530> (**2013**)
- [283] *** <http://www.knmf.kit.edu> Karlsruhe Institute of Technology accessed 20220320
- [284] Pu X, Li G, Huang H. Preparation, anti-biofouling and drag-reduction properties of a biomimetic shark skin surface. *Biology Open*. **2016** Apr 15;5(4):389-96.
- [285] Aizawa T, Suga H, Yamaguchi T. Plasma-nitriding assisted micro-texturing into stainless steel molds. *InMATEC Web of Conferences* **2015** (Vol. 21, p. 09002). EDP Sciences.
- [286] Jiang T, Koch J, Unger C, Fadeeva E, Koroleva A, Zhao Q, Chichkov BN. Ultrashort picosecond laser processing of micro-molds for fabricating plastic parts with superhydrophobic surfaces. *Applied Physics A*. **2012** Sep;108(4):863-9.
- [287] Lutey AH, Lazzini G, Gemini L, Peter A, Onuseit V, Graus J, Fuso F, Kling R, Romoli L. Insight into replication effectiveness of laser-textured micro and nanoscale morphology by injection molding. *Journal of Manufacturing Processes*. **2021** May 1;65:445-54.
- [288] Marinescu MR, Avram M, Voitincu C, Savin M, Mihailescu C, Ghiculescu LD. Electrochemical sensors with interdigitated electrodes for counting T-cells. *SCIENCE AND TECHNOLOGY*. **2020** Jan 1;23(4):368-78.
- [289] Brenner A, Zecherle M, Verpoort S, Schuster K, Schnitzler C, Kogel-Hollacher M, Reisacher M, Nohn B. Efficient production of design textures on large-format 3D mold tools. *Journal of Laser Applications*. **2020** Feb 25;32(1):012018.

Published works

- [401] **Serban D**, Opran CG. Researches regarding injection molding of polymeric products in molds with micro-profiled surfaces. *InIOP Conference Series: Materials Science and Engineering* **2018** August 1 (Vol. 400, No. 3, p. 032009). IOP Publishing. <https://doi.org/10.1088/1757-899x/400/3/032009> WOS:000461147400070
- [402] **Serban D**, Opran CG. Analysis of micro-profile machining of the non-planar surfaces of injection molds for polymeric composites. *Annals of the University of Petroșani*. **2018**;20:99-104. <https://scholar.google.com/scholar?oi=bibs&cluster=12761913127196367403&btnI=1&hl=en> Influ
- [403] **Serban D**, Alexandrescu L, Opran CG. Research Regarding Molding of Fuel Cell Bipolar Plates Made of Polymeric-Carbon Composites. *MSF* **2019**;957:369-78. <https://doi.org/10.4028/www.scientific.net/msf.957.369>.
- [404] **Serban D**, Opran CG. Complex Micro Machining of an Injection Mold Surface for a Conductive Polymeric Composite Product. *In MATEC Web of Conferences* **2019** (Vol. 290, p. 03015). EDP Sciences. <https://doi.org/10.1051/mateconf/201929003015> WOS:000569367700048
- [405] **Serban D**, Lamanna G, Opran CG. Mixing, Conveying and Injection Molding Hybrid System for Conductive Polymer Composites. *Procedia CIRP*. 2019 January 1;81:677-82. <https://doi.org/10.1016/j.procir.2019.03.175> WOS:000566264700116
- [406] **Serban D**, Opran CG. Algorithm for Micro-Profiling from Image of the Injection Molds Complex Surfaces. *In Macromolecular Symposia* **2020** Feb (Vol. 389, No. 1, p. 1900097). <https://doi.org/10.1002/masy.201900097> WOS:000534200700035
- [407] **Serban D**, Opran CG. Injection molded composite bipolar plates for a portable hydrogen fuel cell charger. *In IOP Conference Series: Materials Science and Engineering* **2020** September 1 (Vol. 916, No. 1, p. 012104). IOP Publishing. <https://doi.org/10.1088/1757-899x/916/1/012104> WOS:000625330000104
- [408] **Serban D**, Opran CG. Influence of the Surface Microstructure of Conductive Polymer Composite Bipolar Plate on the Fuel Cell Performance. *In Macromolecular Symposia* **2021** Apr (Vol. 396, No. 1, p. 2000324). <https://doi.org/10.1002/masy.202000324> WOS:000641766900043
- [409] **Serban D**. Influence of Injection Molding Parameters on Electrical Conductivity of Polypropylene-Graphite Composite Bipolar Plates for Hydrogen Fuel Cells. *Mater. Plast.[internet]*. **2021** Jul;58(3):160-173. Available from: <https://doi.org/10.37358/MP.21.3.5514> WOS:000756839200001